

# Hydrated area of a bentonite layer encapsulated between two geomembranes

J. P. Giroud<sup>1</sup>, R. S. Thiel<sup>2</sup> and E. Kavazanjian<sup>3</sup>

<sup>1</sup>Chairman Emeritus, GeoSyntec Consultants, JP GIROUD, INC., 5837 North Ocean Blvd, Ocean Ridge, FL 33435, USA, Telephone: +1 561 737 1642, Telefax: +1 561 733 2809,

E-mail: jpg@jpgiroud.com

<sup>2</sup>Thiel Engineering, PO Box 1010, Oregon House, CA 95962, USA, Telephone: +1 530 692 9114, Telefax +1 530 692 9115, E-mail: richard@rthiel.com

<sup>3</sup>Associate Professor, Department of Civil and Environmental Engineering, Ira J. Fulton School of Engineering, Arizona State University, Tempe, AZ 85287-5306, USA, Telephone: +1 480 727 8566, Telefax: +1 480 965 0557, E-mail: edkavy@aol.com

Received 19 February 2004, revised 29 April 2004, accepted 2 May 2004

**ABSTRACT:** Hydrated bentonite has a low shear strength, which may adversely impact the stability of structures incorporating geosynthetic clay liners (GCLs). Accordingly, in a growing number of GCL applications, the configuration is such that the bentonite layer is encapsulated between two geomembranes in order to reduce the potential for bentonite hydration. This paper considers an encapsulated bentonite layer formed using GM-GCL panels (i.e. panels consisting of a bentonite layer adhered to a carrier geomembrane). The panels are joined by overlapping at the edges and are overlain by a welded geomembrane. Water can migrate from the underlying soil into the bentonite of the overlaps, flow in the bentonite, and migrate laterally in the bentonite between the two geomembranes. Water is driven from the soil to the bentonite by a head difference that results in great part from the suction at the hydration front. This paper presents an analytical method to evaluate the extent of the hydrated area of the bentonite layer as a function of: time, the initial and hydrated moisture content of the bentonite, the hydraulic conductivity of the bentonite, the overlap width, the distance between overlaps, and the head difference. It is important to know the hydrated area for stability calculations. Numerical applications show that, for typical values of the parameters, it takes many decades to hydrate a significant fraction of the bentonite layer area. The analyses presented in this paper also show that, for typical landfill applications, the hydrated area due to leakage through defects in the upper geomembrane is negligible with respect to the hydrated area resulting from water migrating through the overlaps, assuming that the upper geomembrane is installed using good construction quality assurance practices. Uncertainties associated with the methodology presented herein are discussed, and guidance is provided on evaluation of the shear strength of the encapsulated bentonite layer as a function of the shear strength of the unhydrated bentonite, the shear strength of the hydrated bentonite, and the hydrated area.

**KEYWORDS:** Geosynthetics, Geosynthetic clay liner, Geomembrane, Bentonite, Hydration, Hydrated area, Flow, Water, Migration, Containment, Liner system, Barrier, Hydraulic conductivity

**REFERENCE:** Giroud, J. P., Thiel, R. S. & Kavazanjian, E. (2004). Hydrated area of a bentonite layer encapsulated between two geomembranes. *Geosynthetics International*, 11, No. 4, 330–354

## 1. INTRODUCTION

### 1.1. Situation considered

This paper presents a theoretical evaluation of the hydrated area of a layer of bentonite encapsulated between two geomembranes. This configuration is used, in particular, in applications where it is important to retard the development of the hydrated area of the bentonite component of a geosynthetic clay liner (GCL)

owing to water migrating from the underlying soil. This is the case in many waste containment landfills, as the decrease in bentonite shear strength associated with hydration may adversely impact on the stability of the landfill. Therefore it is important to evaluate the extent of the hydrated area, which is the goal of the analysis presented in this paper.

Two types of GCL are currently commercially available in the United States: GCLs where the bentonite

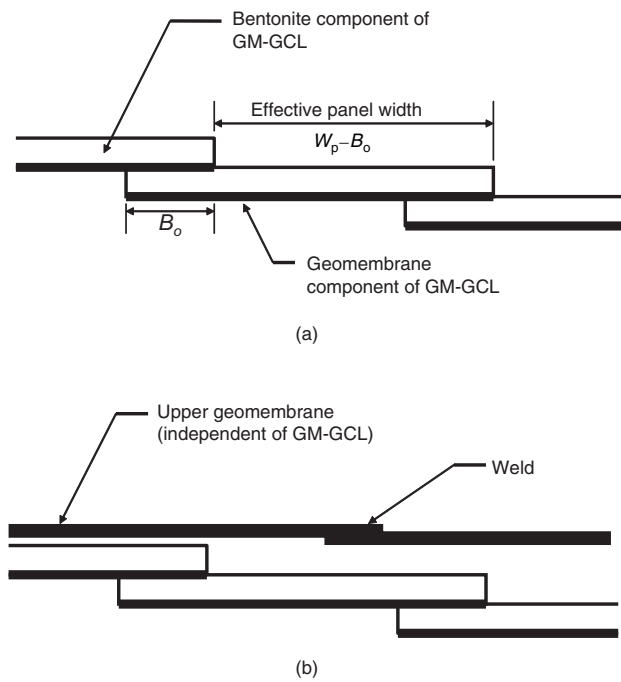


**Figure 1. Schematic representation of overlapped panels of GM-GCL (i.e. a GCL composed of a layer of bentonite and a geomembrane): (a) panels as installed with the geomembrane component down; (b) the same panels covered with an independent geomembrane**

layer is contained between two geotextiles, and GCLs where the bentonite layer is associated with a carrier geomembrane (hereafter designated as GM-GCLs). This paper is devoted to the case where a GM-GCL is placed first, with the bentonite layer up, and a geomembrane is placed on top of the GM-GCL. It is assumed that panels of the GM-GCL are joined simply by overlapping at the edges (Figure 1a). In other words, the geomembrane component of the GM-GCL is not welded. In contrast, the upper geomembrane is assumed to be welded using good construction quality assurance practices.

The GM-GCL panels and the overlying geomembrane form a composite liner (Figure 1b). This configuration is often referred to as a ‘bentonite layer encapsulated between two geomembranes’. In the analyses presented in this paper, the considered composite liner is schematically represented as shown in Figure 2. Among all possible representations of an overlap without wrinkles, the representation used in Figure 2 is conservative with

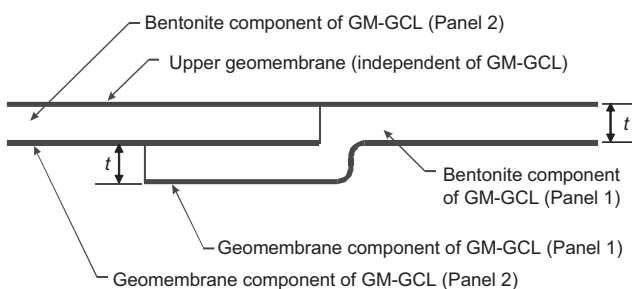


**Figure 2. Schematic representation of a GM-GCL overlap, as used in the analyses**

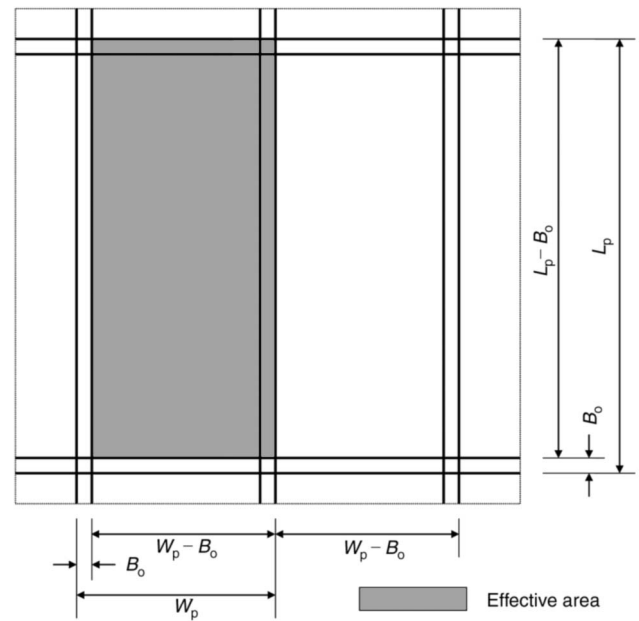


**Figure 3. Effective panel area**

respect to calculating the hydrated area because it maximizes the contact area between the bentonite layer of a GM-GCL panel and the bentonite layer of the adjacent panel, thereby maximizing the potential for water migration in the bentonite.

Figure 3 illustrates the geometry of overlapping GM-GCL panels, wherein:  $B_o$  = overlap width;  $W_p$  = panel width;  $W_p - B_o$  = effective panel width;  $L_p$  = panel length; and  $L_p - B_o$  = effective panel length. The ‘width of the hydrated area’,  $W_H$ , refers to the width of the hydrated area within the effective width of a panel. The effective panel area is defined as follows, based on the effective panel length and the effective panel width:

$$A_p = (W_p - B_o)(L_p - B_o) \tag{1}$$

**1.2. General assumptions**

In the analyses presented in Sections 2 and 3 of this paper, the bentonite layer thickness,  $t$ , is assumed to be uniform. The liquid migrating into the bentonite is assumed to be water or an aqueous solution with hydraulic properties similar to those of water. In particular, the liquid is assumed to be incompressible; therefore mass conservation results in volume conservation.

**1.3. Mechanisms of bentonite hydration**

Hydration of the bentonite will occur when water present in the soil underlying the GM-GCL migrates into the bentonite at the overlaps (Figure 4) and then flows laterally in the bentonite, thereby migrating laterally between the two geomembranes. The bentonite reached by the migrating water becomes hydrated. The surface that separates the hydrated bentonite from the unhydrated bentonite is called the ‘hydration front’. The analyses presented in this paper are consistent with

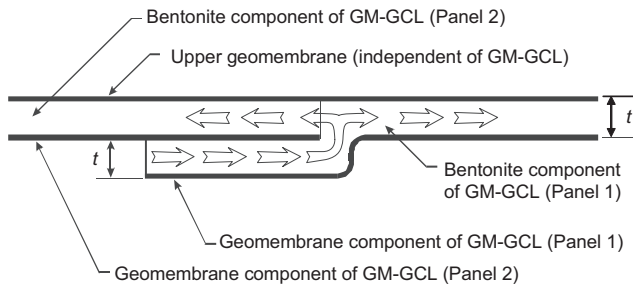


**Figure 4.** Migration of water from the underlying soil into the bentonite layer

the classical Green–Ampt assumption (Green and Ampt 1911) of a well-defined hydration front.

Progressively, as the hydration front migrates into the bentonite, a growing area of the bentonite becomes hydrated. The analyses presented in this paper provide equations for quantifying the area of bentonite hydrated by this mechanism as a function of the following parameters: time, the initial and hydrated moisture content of the bentonite, the thickness of the bentonite layer, the hydraulic conductivity of the bentonite, the overlap width, the distance between overlaps, and the head difference that drives the migration of water.

In addition to the hydration mechanism described above, liquid migrating through geomembrane defects may contribute to the hydration of the bentonite layer. Hydration caused by liquid migrating through geomembrane defects should be superimposed on the hydration caused by water migrating through overlaps of the GM-GCL panels. A methodology for evaluating the hydrated area due to liquid migration through geomembrane defects is proposed in a companion paper by Giroud and Daniel (2004). Calculations using this methodology, presented hereinafter (Section 4.2), show that, for typical landfill applications and a geomembrane installed using good construction quality assurance practices, hydration due to liquid migration through geomembrane defects is negligible compared with hydration due to migration of water through overlaps of the GM-GCL panels. Therefore the hydrated area can be calculated solely by consideration of liquid migration through the overlaps.

Neither hydration by diffusion of water through the geomembranes encapsulating the bentonite layer nor hydration by diffusion of water vapor through the bentonite is considered in this paper. These two restrictions are discussed in detail in the companion paper (Giroud & Daniel 2004), where it is shown that they do not affect the validity of the methodology presented herein.

## 1.4. Driving head

### 1.4.1. Head difference

The lateral migration of liquid in the bentonite is driven by the head difference,  $\Delta h$ , between the suction head at the hydration front (making the classical Green–Ampt assumption (Green and Ampt 1911) of a distinct, well-defined hydration front) and the head at the location where the liquid migrates into the bentonite. The head

difference depends on the source of hydration: either migration of water from the soil underlying the lower geomembrane or migration of liquid initially contained above the upper geomembrane. These two cases are addressed in the following sections.

It should be noted that, while the equations presented below for the driving head are based upon the assumption of a well-defined hydration front, Giroud and Daniel (2004) show that they are valid approximations for the case where the hydration front is in fact a diffuse hydration zone.

### 1.4.2. Driving head in case of water migrating from the soil underlying the lower geomembrane

In the case of migration of water from the soil underlying the lower geomembrane, the lateral migration of water in the bentonite is driven by the difference between the head at the bentonite hydration front and the head in the soil underlying the lower geomembrane. For unsaturated porous materials, such as unsaturated bentonite or soil, a negative head may exist due to suction. Therefore the head difference that drives water migration,  $\Delta h$ , can be expressed as follows:

$$\Delta h = s_b - s_s \quad (2)$$

where  $s_b$  = suction head in the bentonite at the hydration front; and  $s_s$  = suction head in the soil underlying the lower geomembrane. While the suction head represents a negative porewater pressure,  $s_b$  and  $s_s$  are positive numbers (i.e.  $s_b$  and  $s_s$  are  $> 0$ ). Equation 2 and the terminology ‘suction head’ imply that suction is expressed in units of head, not in units of pressure.

There are some cases where there is a positive porewater pressure in the soil underlying the lower geomembrane. This happens, for example, in the case of landfill liners located below the groundwater table. In these cases, the head difference that drives water migration,  $\Delta h$ , can be expressed as follows:

$$\Delta h = s_b + h_s \quad (3)$$

where  $h_s$  = pressure head in the soil underlying the lower geomembrane.

### 1.4.3. Driving head in case of leakage through a defect in the upper geomembrane

In the case of liquid leaking through a defect in the upper geomembrane, the head difference,  $\Delta h$ , results from the suction head at the hydration front,  $s_b$ , and the head of liquid above the geomembrane defect,  $h_w$ . It is expressed as follows:

$$\Delta h = s_b + h_w \quad (4)$$

### 1.4.4. Typical values

A detailed discussion of the values of the parameters of Equations 2 to 4 is presented in the companion paper (Giroud and Daniel 2004), where it is recommended to use  $s_b = 3$  m in conjunction with the use of the saturated hydraulic conductivity for the hydraulic conductivity of the hydrated bentonite in design calculations for water migration in encapsulated bentonite layers. This recommendation is based, in part, upon back-analyses of

hydration front migration observed in the field and laboratory. It must be noted that the hydration front migration rate depends upon the product of the head difference (between hydration front and underlying soil) and the hydraulic conductivity of hydrated bentonite (Giroud and Daniel 2004). Therefore, if the hydrated bentonite is not saturated and the hydraulic conductivity is therefore less than the saturated hydraulic conductivity (see Section 1.5.3), the suction head at the hydration front may be greater than the value determined from back-analyses using the saturated hydraulic conductivity. However, based upon agreement between observed and calculated hydration front migration rates reported by Giroud and Daniel (2004), the use of a 3 m suction head at the hydration front in conjunction with the saturated hydraulic conductivity of bentonite is considered an appropriate engineering assumption for the analyses developed herein. This important point is discussed again in Section 5.4.

Soil suction head,  $s_s$ , typically varies between 0 m (coarse-grained soils or saturated fine-grained soils) and 1 m (dry fine-grained soils), according to Estornell and Daniel (1992). In the case of liners that are below the groundwater table, the pressure head in the soil beneath the GM-GCL overlaps,  $h_s$ , can have any value, as dictated by the local conditions.

In landfills, the head of liquid above the upper geomembrane defect,  $h_w$ , is generally less than 0.3 m, whereas in liquid impoundments  $h_w$  is generally several meters.

### 1.5. Bentonite layer characteristics

A detailed discussion of the bentonite layer characteristics is presented in the companion paper (Giroud and Daniel 2004). This discussion is summarized below.

#### 1.5.1. Thickness of the bentonite layer

The initial moisture content and the initial thickness of the bentonite layer are assumed to have the values they have in the GCL as manufactured (e.g. 15–25%). In GCLs typically used in the United States, the initial thickness is approximately 6 mm.

Some time after installation the GCL is subjected to overburden pressure, as the overlying structure (e.g. landfill) is being built and/or filled. It is assumed herein that hydration occurs after application of the overburden pressure. As the GCL is subjected to overburden pressure and hydration, it may shrink or swell depending on the interplay between overburden-induced compression and hydration-induced swell. As a result, the bentonite layer thickness after hydration may be smaller or greater than the initial thickness.

A detailed discussion presented by Giroud and Daniel (2004) shows that the analysis of hydration should be conducted using the bentonite layer thickness that corresponds to the overburden pressure applied to hydrated bentonite (and not the initial thickness). An approximate relationship between hydrated bentonite layer thickness and overburden pressure is presented in the first two columns of Table 1. Although it is preferable to have actual data for the specific bentonite layer used in a given project, this approximate relationship can be used for bentonite layers having a dry mass per unit area of the order of 3.9–4.4 kg/m<sup>2</sup> (0.8–0.9 lb/ft<sup>2</sup>). This includes bentonite layers found in GCLs currently used in the United States.

#### 1.5.2. Hydration volumetric content of the bentonite

The volumetric content of hydration water,  $\theta_{\text{hydr}}$ , hereafter called ‘hydration volumetric content’, is a dimensionless parameter that quantifies the amount of water used to hydrate the encapsulated bentonite. The hydration volumetric content is defined as the ratio between: (i) the volume of water added to the bentonite between the initial state and the hydrated state; and (ii) the total volume of the hydrated bentonite.

A detailed analysis and a parametric study presented in Appendix 1 show that, for typical values of the initial moisture content of the bentonite in GCLs used in the United States (15–25%), the initial moisture content does not have a significant influence on the value of the hydration volumetric content if the bentonite degree of saturation following hydration is greater than 0.8. Considering a degree of saturation of the hydrated bentonite of 0.8–0.9, the parametric study leads to the

**Table 1. Typical properties of bentonite layer relevant to design (for dry mass per unit area of the order of 3.9–4.4 kg/m<sup>2</sup> (0.8–0.9 lb/ft<sup>2</sup>) and initial moisture content ranging between 15% and 25%)**

Overburden pressure (kPa)	Thickness of hydrated bentonite layer, $t_h$ (mm)	Hydration volumetric content of hydrated bentonite, $\theta_{\text{hydr}}$ (dimensionless)	Hydraulic conductivity of saturated bentonite, $k$ (m/s)
10	8.0	0.50	$5 \times 10^{-11}$
50	7.0	0.45	$3 \times 10^{-11}$
100	6.0	0.40	$2 \times 10^{-11}$
200	5.0	0.35	$1 \times 10^{-11}$
400	4.0	0.25	$2 \times 10^{-12}$
500	3.5	0.15	$1 \times 10^{-12}$

Notes: The hydration volumetric content was determined assuming a degree of saturation of the hydrated bentonite,  $S_h$ , of 0.8–0.9. For different values of  $S_h$ ,  $\theta_{\text{hydr}}$  would be different. In particular, for  $S_h < 0.8$ ,  $\theta_{\text{hydr}}$  would be smaller than shown in the table. The first two columns are based on data from Shan (1993), the relationship between the second and third columns is from a parametric study presented in Appendix 1, and the relationship between the first and fourth columns is based on data from Daniel (1996).

relationship between the hydration volumetric content and the thickness of the hydrated bentonite layer presented in the second and third columns of Table 1. This relationship can be used for bentonite layers having a dry mass per unit area of the order of 3.9–4.4 kg/m<sup>2</sup> (0.8–0.9 lb/ft<sup>2</sup>). For other bentonite layers and/or other degrees of saturation, the hydration volumetric content can be calculated as shown in Appendix 1.

### 1.5.3. Hydraulic conductivity of the bentonite

The velocity of hydration front migration is dependent on the hydraulic conductivity of the hydrated bentonite, because the path over which the liquid migrates is in the hydrated bentonite. The hydraulic conductivity of the bentonite depends on the degree of saturation of the bentonite and the overburden pressure.

The hydraulic conductivity of bentonite increases with increasing values of the degree of saturation. The hydrated bentonite may not be completely saturated. In numerical applications, it might seem conservative (with respect to the rate of hydration) to use, for the hydrated bentonite, the hydraulic conductivity of saturated bentonite, because the hydraulic conductivity of unsaturated bentonite is less than or equal to (but never greater than) the hydraulic conductivity of saturated bentonite if all other factors are held constant. However, as discussed in Section 1.4.4, for the analyses presented herein, the selection of the hydraulic conductivity is linked to the value selected for the suction head at the hydration front. Thus, for the analyses presented herein, if a suction head of 3 m is assumed for the hydration front, the use of the saturated hydraulic conductivity for the bentonite behind the hydration front is neither conservative nor unconservative, but merely should be considered appropriate.

The hydraulic conductivity of saturated bentonite decreases with increasing values of the overburden pressure. An approximate relationship between overburden pressure and hydraulic conductivity of saturated bentonite used in GCLs in the United States is presented in the first and last columns of Table 1. Table 1 shows that there is a large difference between the hydraulic conductivity value ( $k = 5 \times 10^{-11}$  m/s) for 10 kPa overburden pressure (representative of a landfill cover) and the hydraulic conductivity ( $k = 1 \times 10^{-12}$  m/s) for 500 kPa (representative of a landfill liner overlain by approximately 40 m of waste). As shown subsequently, this difference in hydraulic conductivity leads to a substantial difference in hydration rates for representative liner and cover systems.

### 1.6. Organisation of this paper

Section 2 presents equations for hydration due to water migrating through overlaps of the GM-GCL panels, Section 3 presents an equation for the hydrated area due to liquid migrating through geomembrane defects, Section 4 summarizes design equations and presents design examples, Section 5 presents a discussion of the influence of parameters, and Section 6 discusses the

impact of the hydrated area on shear strength and stability.

## 2. HYDRATION DUE TO WATER MIGRATING THROUGH GM-GCL PANEL OVERLAPS

### 2.1. Assumptions

It is assumed that the hydration front is planar (i.e. the Green–Ampt assumption mentioned in Sections 1.3 and 1.4.1) and migrates one-dimensionally in the direction perpendicular to the overlap length. Overlaps are present at both sides and at both ends of each GM-GCL panel. Therefore the hydration of a given panel proceeds simultaneously from both sides and both ends of the panel. Based on the assumption of one-dimensional migration of a planar hydration front, the panel area that is not hydrated (referred to as the ‘unhydrated’ area and not the ‘dry’ area because, in this area, the bentonite is not perfectly dry) is perfectly rectangular (i.e. with right-angle corners; Figure 5). It is likely that, in reality, the unhydrated area has rounded corners (simply because hydration is faster in corners, as it proceeds in two directions rather than one). Since panel length is usually large compared with panel width, the approximation that results from neglecting rounded corners is deemed acceptable for typical applications.

### 2.2. Phases of water migration

Three distinct phases can be considered as migration of water from the underlying soil progresses in the bentonite layer. These phases are illustrated in Figure

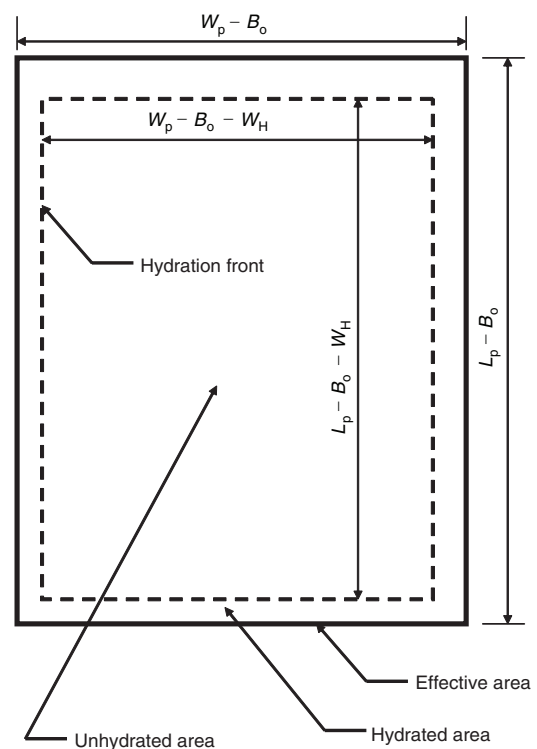


Figure 5. Hydration front, hydrated area and unhydrated area

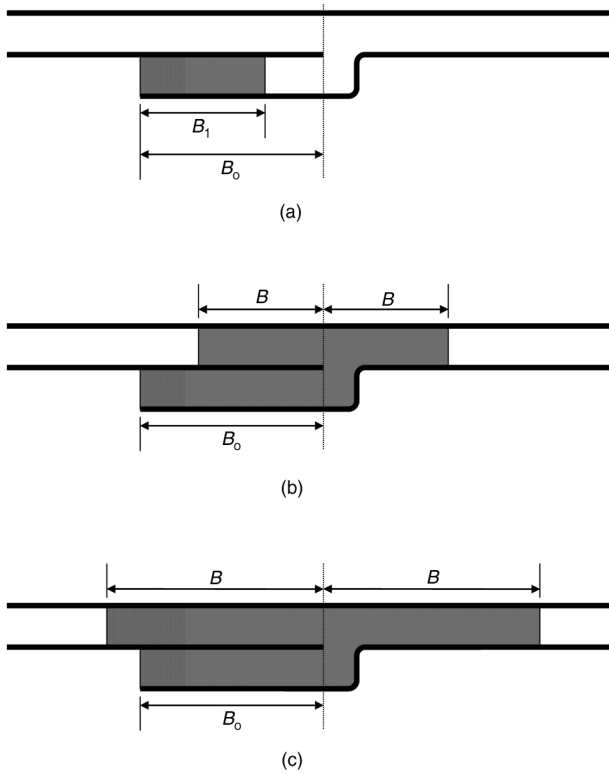


Figure 6. The three phases of water migration from the underlying soil: (a) Phase 1; (b) Phase 2; (c) Phase 3

6. In each phase, the expression for the width of the hydrated area,  $W_H$ , is different (Figure 7).

2.2.1. First phase (Phase 1)

The first phase is when the hydration front is still in the overlap (Figures 6a and 7a). This phase is defined by

$$B_1 \leq B_0 \tag{5}$$

where  $B_1$  is the width of bentonite within the overlap that is hydrated at a given time during Phase 1.

In the first phase, the width of the hydrated area related to one panel (Figure 7a) is given by

$$W_H = B_1 \tag{6}$$

The first phase ends when the migrating water has hydrated the full width of the overlap, i.e. when

$$W_H = B_1 = B_0 \tag{7}$$

2.2.2. Second phase (Phase 2)

The second phase (Figures 6b and 7b) is defined by

$$0 \leq B \leq B_0 \tag{8}$$

where  $B$  is the distance reached by water beyond the overlap.

In the second phase, the width of the hydrated area related to one panel (Figure 7b) is given by

$$W_H = B_0 + B \tag{9}$$

The second phase ends when

$$B = B_0 \tag{10}$$

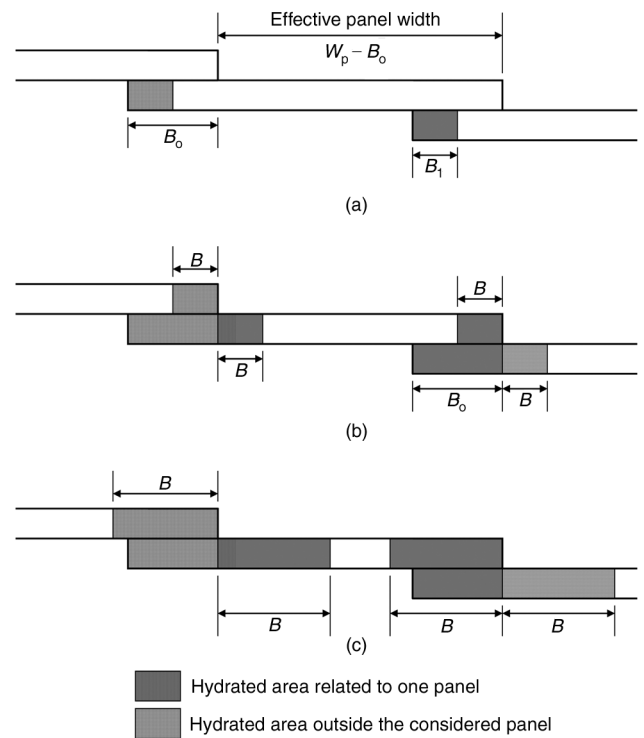


Figure 7. Width of hydrated area: (a) Phase 1; (b) Phase 2; (c) Phase 3 [Note: the geomembrane component of the GM-GCL is not shown for the sake of clarity]

From Equations 9 and 10, the width of the hydrated area at the end of Phase 2 is

$$W_H = 2B_0 \tag{11}$$

2.2.3. Third phase (Phase 3)

The third phase (Figures 6c and 7c) is defined by

$$B_0 \leq B \leq \frac{W_P - B_0}{2} \tag{12}$$

In the third phase, the width of the hydrated area related to one panel (Figure 7c) is given by

$$W_H = 2B \tag{13}$$

The third phase ends when the bentonite layer is entirely hydrated, which happens when the width of the hydrated area is equal to the effective panel width:

$$W_H = 2B = W_P - B_0 \tag{14}$$

2.3. Extent of the hydrated area

2.3.1. Hydrated area

Based on Figure 5, the hydrated area of the considered panel,  $A_H$ , is

$$A_H = A_P - A_U \tag{15}$$

where:  $A_H$  = hydrated area of the panel;  $A_P$  = effective area of the panel (Figures 3 and 5); and  $A_U$  = unhydrated area of the panel.

The unhydrated area of the considered panel (Figure 5) is

$$A_U = (W_P - B_0 - W_H)(L_P - B_0 - W_H) \tag{16}$$

Combining Equations 1, 15 and 16 gives the hydrated area of the considered panel as follows:

$$A_H = W_H(W_P + L_P - 2 B_o) - W_H^2 \tag{17}$$

2.3.2. *Relative hydrated area*

The relative hydrated area is defined as the ratio between the hydrated area of a panel and the effective panel area:

$$R_{HA} = \frac{A_H}{A_P} \tag{18}$$

Combining Equations 1, 17 and 18 gives:

$$R_{HA} = \frac{W_H}{W_P - B_o} + \frac{W_H}{L_P - B_o} - \left( \frac{W_H}{W_P - B_o} \right) \left( \frac{W_H}{L_P - B_o} \right) \tag{19}$$

Equation 19 is valid for all three phases of water migration, but the value of  $W_H$  depends on the phase, as indicated in Section 2.2. The value of  $W_H$  is given by Equation 6 for Phase 1, by Equation 7 for the end of Phase 1, by Equation 9 for Phase 2, by Equation 11 for the end of Phase 2, by Equation 13 for Phase 3, and by Equation 14 for the end of Phase 3.

2.3.3. *Relative hydrated area at the end of Phase 1*

Combining Equations 7 and 19 gives the relative hydrated area at the end of Phase 1 (i.e. at the Interphase 1-2) as follows:

$$R_{HA1-2} = \frac{B_o}{W_P - B_o} + \frac{B_o}{L_P - B_o} - \frac{B_o^2}{(W_P - B_o)(L_P - B_o)} \tag{20}$$

2.3.4. *Relative hydrated area at the end of Phase 2*

Combining Equations 11 and 19 gives the relative hydrated area at the end of Phase 2 (i.e. at the Interphase 2-3) as follows:

$$R_{HA2-3} = \frac{2B_o}{W_P - B_o} + \frac{2B_o}{L_P - B_o} - \frac{4B_o^2}{(W_P - B_o)(L_P - B_o)} \tag{21}$$

2.3.5. *Relative hydrated area at the end of Phase 3*

Combining Equations 14 and 19 gives the relative hydrated area at the end of Phase 3:

$$R_{HAend} = 1.00 = 100\% \tag{22}$$

Obviously, at the end of Phase 3, the bentonite is hydrated over the entire panel.

2.4. **Analysis of water migration**

2.4.1. *Phase 1*

During Phase 1 (i.e. in the case illustrated in Figures 6a and 7a), Darcy's equation can be written as follows:

$$\frac{Q}{L} = k i_1 \left( \frac{A}{L} \right) \tag{23}$$

where:  $Q/L$  = rate of liquid migration per unit length perpendicular to the plane of Figure 6 or 7;  $k$  = hydraulic conductivity of the hydrated bentonite, hereafter referred to as the 'hydraulic conductivity of the bentonite';  $i_1$  = hydraulic gradient in Phase 1;  $A$  = cross-sectional area through which liquid is migrating; and

$A/L$  = cross-sectional area through which liquid is migrating, per unit length perpendicular to the plane of Figure 6 or 7.

The cross-sectional area through which liquid is migrating, per unit length perpendicular to the plane of Figure 6 or 7, is

$$\frac{A}{L} = t \tag{24}$$

where  $t$  is the thickness of the bentonite layer.

At a given time,  $\hat{t}$ , the hydraulic gradient,  $i_1$ , is given by

$$i_1 = \frac{\Delta h}{B_1} \tag{25}$$

Combining Equations 23 to 25 gives

$$\frac{Q}{L} = \frac{k t \Delta h}{B_1} \tag{26}$$

The volume of water that has been used to hydrate the bentonite between time zero ( $\hat{t} = 0$ ) and time  $\hat{t}$  per unit length perpendicular to the plane of Figure 6 or 7 is

$$\frac{V}{L} = \theta_{hydr} t B_1 \tag{27}$$

where  $\theta_{hydr}$  is the hydration volumetric content defined in Section 1.5.2.

Since the rate of liquid migration,  $Q$ , is the derivative of the volume with respect to time, volume conservation is expressed as follows, based on Equation 27:

$$\frac{Q}{L} = \frac{1}{L} \frac{dV}{d\hat{t}} = \theta_{hydr} t \frac{dB_1}{d\hat{t}} \tag{28}$$

Eliminating  $Q/L$  between Equations 26 and 28 gives

$$d\hat{t} = \frac{\theta_{hydr}}{k \Delta h} B_1 dB_1 \tag{29}$$

Integration of Equation 29 (with  $\hat{t} = 0$  for  $B_1 = 0$  and using the notation  $\hat{t} = \hat{t}_1$  for Phase 1) gives

$$\hat{t}_1 = \frac{\theta_{hydr}}{2k \Delta h} B_1^2 \tag{30}$$

2.4.2. *Interphase 1-2*

The end of Phase 1, which is also the beginning of Phase 2, occurs when  $B_1 = B_o$ , which happens at time  $\hat{t}_{1-2}$  given by the following equation derived from Equation 30:

$$\hat{t}_{1-2} = \frac{\theta_{hydr} B_o^2}{2k \Delta h} \tag{31}$$

2.4.3. *Phases 2 and 3*

At the end of Phase 1, when the hydration front reaches the end of the overlap, it bifurcates. As a result, the flow is shared between two GM-GCL panels (Figures 4, 6b and 6c). Therefore the total bentonite thickness available for flow is  $t$  for the portion of flow in the overlap, and  $2t$  after the overlap. Owing to volume conservation, and assuming that the degree of saturation, while not necessarily 100%, remains constant behind the hydration front, the sum of the flow rates in the two sections of

length  $B$  after the overlap is the same as the flow rate in the overlap; hence, based on Darcy's equation:

$$\frac{Q}{L} = ki_o \frac{A_o}{L} = ki_e \frac{A_e}{L} \tag{32}$$

where:  $i_o$  = hydraulic gradient in the overlap;  $i_e$  = hydraulic gradient in the bentonite section hydrated beyond the overlap;  $A_o$  = cross-sectional area through which liquid is migrating in the overlap;  $A_o/L$  = cross-sectional area through which liquid is migrating in the overlap, per unit length perpendicular to the plane of Figure 6 or 7;  $A_e$  = cross-sectional area through which liquid is migrating beyond the overlap; and  $A_e/L$  = cross-sectional area through which liquid is migrating beyond the overlap, per unit length perpendicular to the plane of Figure 6 or 7.

As indicated above, the total bentonite thickness available for flow is  $t$  for the portion of flow in the overlap, and  $2t$  after the overlap. Hence:

$$\frac{A_o}{L} = t \tag{33}$$

and

$$\frac{A_e}{L} = 2t \tag{34}$$

The hydraulic gradient is defined as the ratio between head loss and flow length. Hence:

$$i_o = \frac{\Delta h_o}{B_o} \tag{35}$$

and

$$i_e = \frac{\Delta h_e}{B} \tag{36}$$

where:  $\Delta h_o$  = head loss in the overlap; and  $\Delta h_e$  = head loss in the bentonite section hydrated beyond the overlap.

The following relationship exists between the unknown head losses  $\Delta h_o$  and  $\Delta h_e$  and the known head difference,  $\Delta h$ :

$$\Delta h_o + \Delta h_e = \Delta h \tag{37}$$

Combining Equations 32 to 37 gives

$$i_o = 2i_e = \frac{2\Delta h}{B + 2B_o} \tag{38}$$

Combining Equations 32, 33 and 38 gives

$$\frac{Q}{L} = \frac{2kt\Delta h}{B + 2B_o} \tag{39}$$

During Phases 2 and 3, the change in water volume stored in the bentonite layer occurs in the encapsulated portion. Therefore it is expressed by

$$dV = 2\theta_{hydr}tLdB \tag{40}$$

Since the rate of liquid migration,  $Q$ , is the derivative of the volume with respect to time, volume conservation is expressed as follows, based on Equation 40:

$$Q = \frac{dV}{dt} = 2\theta_{hydr}tL \frac{dB}{dt} \tag{41}$$

Combining Equations 39 and 41 gives

$$\frac{2kt\Delta h}{B + 2B_o} = 2\theta_{hydr}t \frac{dB}{dt} \tag{42}$$

Hence:

$$d\hat{t} = \frac{\theta_{hydr}}{k\Delta h} (B + 2B_o)dB \tag{43}$$

Integration of Equation 43 (with  $\hat{t} = \hat{t}_{1-2}$  for  $B = 0$ ), and using the notation  $\hat{t} = \hat{t}_2$  for Phase 2 and  $\hat{t} = \hat{t}_3$  for Phase 3, gives

$$\hat{t}_2 = \hat{t}_3 = \hat{t}_{1-2} + \frac{\theta_{hydr}B^2}{k\Delta h} \left( \frac{1}{2} + \frac{2B_o}{B} \right) \tag{44}$$

Combining Equations 31 and 44 gives

$$\hat{t}_2 = \hat{t}_3 = \frac{\theta_{hydr}}{2k\Delta h} (B_o^2 + B^2 + 4BB_o) \tag{45}$$

#### 2.4.4. Interphase 2-3

For the limit case between the second and third phases, combining Equations 10 and 45 gives

$$\hat{t}_{2-3} = \frac{3\theta_{hydr}B_o^2}{k\Delta h} = 6\hat{t}_{1-2} \tag{46}$$

#### 2.4.5. End of Phase 3

At the end of the third phase (i.e. when the entire bentonite area is hydrated), combining Equations 14 and 45 gives

$$\begin{aligned} \hat{t}_{end} &= \frac{\theta_{hydr}}{8k\Delta h} (W_P^2 + 6W_P B_o - 3B_o^2) \\ &= \frac{\theta_{hydr}}{2k\Delta h} \left[ \left( \frac{W_P + B_o}{2} \right)^2 + B_o(W_P - B_o) \right] \end{aligned} \tag{47}$$

where  $\hat{t}_{end}$  is the time at which the entire bentonite layer is hydrated, which marks the end of Phase 3.

#### 2.4.6. General comment

Equations 30, 31, 45, 46 and 47 show that the time required for the liquid to reach a certain distance is independent of the bentonite layer thickness.

### 2.5. Calculation of the relative hydrated area

#### 2.5.1. Principle of calculation

The equations presented in Section 2.3 give the time required for the hydration front to reach a certain distance from the edge of the panel. Hereafter, these equations are combined with equations presented in Sections 2.1 and 2.2 to obtain the relative hydrated area as a function of time.

#### 2.5.2. Equations for Phase 1

Equations 6 and 30 give the following relationship, valid in Phase 1 only:

$$W_H = B_1 = \sqrt{\frac{2k\hat{t}\Delta h}{\theta_{hydr}}} \tag{48}$$

Combining Equations 19 and 48 gives the following direct relationship between the relative hydrated area and time for the first phase:

$$R_{HA1} = \frac{\sqrt{\frac{2k\hat{t}\Delta h}{\theta_{hydr}} \left( \frac{1}{W_P - B_o} + \frac{1}{L_P - B_o} \right)} - \frac{2k\hat{t}\Delta h}{\theta_{hydr}(W_P - B_o)(L_P - B_o)}}{1} \quad (49)$$

2.5.3. Equations common to Phases 2 and 3

Equation 45 (which is valid in both Phases 2 and 3) can be written as follows:

$$B^2 + 4BB_o + B_o^2 - \frac{2k\hat{t}\Delta h}{\theta_{hydr}} = 0 \quad (50)$$

Equation 50 is a quadratic equation for the variable *B*. The positive solution of this equation is

$$B = \sqrt{3B_o^2 + \frac{2k\hat{t}\Delta h}{\theta_{hydr}}} - 2B_o \quad (51)$$

Since Equation 51 was derived from Equation 45, it is valid for both the second and third phases.

2.5.4. Equations for Phase 2

Combining Equations 9 and 51 gives the following equation for the width of the hydrated area in Phase 2:

$$W_H = B_o + B = \sqrt{3B_o^2 + \frac{2k\hat{t}\Delta h}{\theta_{hydr}}} - B_o \quad (52)$$

Combining Equations 19 and 52 gives the following direct relationship between the relative hydrated area and time for the second phase:

$$R_{HA2} = \frac{\left( \sqrt{3B_o^2 + \frac{2k\hat{t}\Delta h}{\theta_{hydr}}} - B_o \right) \times \left( \frac{1}{W_P - B_o} + \frac{1}{L_P - B_o} \right) - \frac{\left( \sqrt{3B_o^2 + \frac{2k\hat{t}\Delta h}{\theta_{hydr}}} - B_o \right)^2}{(W_P - B_o)(L_P - B_o)}}{1} \quad (53)$$

2.5.5. Equations for Phase 3

Combining Equations 13 and 51 gives the following equation for the width of the hydrated area in Phase 3:

$$W_H = 2B = 2\sqrt{3B_o^2 + \frac{2k\hat{t}\Delta h}{\theta_{hydr}}} - 4B_o \quad (54)$$

Combining Equations 19 and 54 gives the following direct relationship between the relative hydrated area and time for the third phase:

$$R_{HA3} = \frac{\left( 2\sqrt{3B_o^2 + \frac{2k\hat{t}\Delta h}{\theta_{hydr}}} - 4B_o \right) \times \left( \frac{1}{W_P - B_o} + \frac{1}{L_P - B_o} \right) - \frac{\left( 2\sqrt{3B_o^2 + \frac{2k\hat{t}\Delta h}{\theta_{hydr}}} - 4B_o \right)^2}{(W_P - B_o)(L_P - B_o)}}{1} \quad (55)$$

**3. HYDRATED AREA DUE TO LIQUID MIGRATION THROUGH GEOMEMBRANE DEFECTS**

**3.1. Presentation of the case**

Composite liners that consist of a GM-GCL overlain by a welded geomembrane are used to contain a liquid, such as water or leachate. If there is a defect in the upper geomembrane, some of the liquid initially contained above the upper geomembrane migrates into the bentonite. Similarly, if there is a defect in the lower geomembrane, some of the liquid initially contained in the soil underlying the lower geomembrane migrates into the bentonite. The liquid that has migrated into the bentonite then migrates laterally in the bentonite between the two geomembranes. The liquid that migrates laterally in the bentonite layer hydrates a fraction of the bentonite layer. Analyses presented by Giroud and Daniel (2004) lead to an equation for quantifying the area of bentonite layer hydrated by liquid migrating through a geomembrane defect. This area should be added to the area hydrated by liquid migrating through overlaps of the GM-GCL panels. However, calculations presented in Section 4.2 will show that, for typical landfill applications, the area hydrated by liquid migrating through geomembrane defects is negligible compared with the area hydrated by liquid migrating through overlaps of the GM-GCL panels, assuming that the frequency and size of defects are representative of geomembrane liner installed with good construction quality assurance practices, as described in Section 1.5 of the companion paper (Giroud and Daniel 2004).

**3.2. Equation for hydrated area due to liquid migration through geomembrane defects**

Giroud and Daniel (2004) developed equations for the case of liquid migrating through a circular defect of radius *r* and then migrating radially in the bentonite layer. The case where the defect is in the upper geomembrane is illustrated in Figure 8. At time *t̂*, the migrating liquid is assumed to have reached a radial distance *R* from the center of the defect, thereby forming an axisymmetrical cylindrical hydration front. The following equation was developed by Giroud and Daniel (2004) for the bentonite hydrated area due to liquid

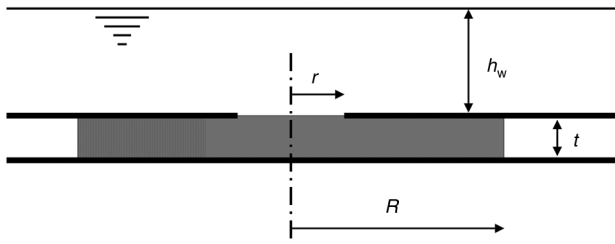


Figure 8. Bentonite hydration due to liquid leaking through a defect in the upper geomembrane

migrating through a defect in one of the geomembranes encapsulating a bentonite layer:

$$\left(\frac{4\pi k \Delta h}{\theta_{hydr} a}\right) \hat{t} - 1 = \left(\frac{A_{Hdef}}{a}\right) \left[\ln\left(\frac{A_{Hdef}}{a}\right) - 1\right] \quad (56)$$

where  $\Delta h$  is given by Equation 2 or 3 (in the case of defects in the lower geomembrane) or Equation 4 (in the case of defects in the upper geomembrane),  $A_{Hdef}$  is the surface area of the circular hydrated area of radius  $R$  due to liquid migrating through a geomembrane defect, and  $a$  is the circular defect area.

Equation 56 can be solved by iterations to give the hydrated area as a function of the other parameters, as shown in Example 2 (Section 4.2). Then the relative hydrated area due to liquid migrating through defects can be calculated using the following equation:

$$R_{HAdef} = \frac{N A_{Hdef}}{A_{unit}} \quad (57)$$

where  $N$  is the number of defects in the unit area,  $A_{unit}$ . It is important to express  $A_{Hdef}$  and  $A_{unit}$  using the same units. For example, if there are five defects per hectare, and if  $A_{Hdef}$  is expressed in  $m^2$ ,  $N = 5$  and  $A_{unit} = 10,000 m^2$ ; or if there are two defects per acre, and if  $A_{Hdef}$  is expressed in  $ft^2$ ,  $N = 2$  and  $A_{unit} = 43,560 ft^2$ .

## 4. DESIGN EQUATIONS AND DESIGN EXAMPLES

### 4.1. Design equations, assumptions and parameters

#### 4.1.1. Rigorous equations

The equations required for performing design calculations are scattered in various sections of this paper. In order to provide design engineers with a practical tool, all of the useful equations are presented together in Table 2 for the width of the hydrated area and Table 3 for the relative hydrated area.

#### 4.1.2. Approximate equations for the relative hydrated area

In many practical cases,  $B_o$  is small with respect to  $W_P$ , and  $W_P$  is small with respect to  $L_P$ . In those cases, the equations of the relative hydrated area presented in Table 3 reduce to the following equations respectively:

$$R_{HA1} \approx \frac{1}{W_P} \sqrt{\frac{2k \hat{t} \Delta h}{\theta_{hydr}}} \quad (58)$$

$$R_{HA1-2} \approx \frac{B_o}{W_P} \quad (59)$$

$$R_{HA2} \approx \frac{1}{W_P} \left( \sqrt{3B_o^2 + \frac{2k \hat{t} \Delta h}{\theta_{hydr}}} - B_o \right) \quad (60)$$

$$R_{HA2-3} \approx \frac{2B_o}{W_P} \approx 2R_{HA1-2} \quad (61)$$

$$R_{HA3} \approx \frac{2}{W_P} \left( \sqrt{3B_o^2 + \frac{2k \hat{t} \Delta h}{\theta_{hydr}}} - 2B_o \right) \quad (62)$$

Equations 58 to 62 underestimate the value of the relative hydrated area. A dimensionless factor,  $C_{RHA}$ , can be used as follows to improve the approximation:

$$R_{HA1} \approx C_{RHA} \frac{1}{W_P} \sqrt{\frac{2k \hat{t} \Delta h}{\theta_{hydr}}} \quad (63)$$

$$R_{HA1-2} \approx C_{RHA} \frac{B_o}{W_P} \quad (64)$$

Table 2. Equations for width of the hydrated area due to water migration from the underlying soil through the GM-GCL panel overlaps

Phase	Equation for the width of the hydrated area
Phase 1	$W_{H1} = \sqrt{\frac{2k \hat{t} \Delta h}{\theta_{hydr}}} \quad (48)$
End of Phase 1 (Interphase 1-2)	$W_{H1-2} = B_o \quad (7)$
Phase 2	$W_{H2} = \sqrt{3B_o^2 + \frac{2k \hat{t} \Delta h}{\theta_{hydr}}} - B_o \quad (52)$
End of Phase 2 (Interphase 2-3)	$W_{H2-3} = 2B_o = 2W_{H1-2} \quad (11)$
Phase 3	$W_{H3} = 2\sqrt{3B_o^2 + \frac{2k \hat{t} \Delta h}{\theta_{hydr}}} - 4B_o \quad (54)$
End of Phase 3	$W_{Hend} = W_P - B_o \quad (14)$

Note:  $\Delta h$  is given by Equation 2, 3 or 4.

**Table 3. Equations for relative hydrated area and time for bentonite hydration due to water migration from the underlying soil through the GM-GCL panel overlaps**

Phase	Equation
Phase 1	$R_{HA1} = \sqrt{\frac{2k\hat{t}\Delta h}{\theta_{hydr}} \left( \frac{1}{W_P - B_o} + \frac{1}{L_P - B_o} \right)} - \frac{2k\hat{t}\Delta h}{\theta_{hydr}(W_P - B_o)(L_P - B_o)}$ (49)
End of Phase 1	$R_{HA1-2} = \frac{B_o}{W_P - B_o} + \frac{B_o}{L_P - B_o} - \frac{B_o^2}{(W_P - B_o)(L_P - B_o)}$ (20)
	$\hat{t}_{1-2} = \frac{\theta_{hydr} B_o^2}{2k\Delta h}$ (31)
Phase 2	$R_{HA2} = \left( \sqrt{3B_o^2 + \frac{2k\hat{t}\Delta h}{\theta_{hydr}}} - B_o \right) \left( \frac{1}{W_P - B_o} + \frac{1}{L_P - B_o} \right) - \frac{\left[ \sqrt{3B_o^2 + (2k\hat{t}\Delta h/\theta_{hydr})} - B_o \right]^2}{(W_P - B_o)(L_P - B_o)}$ (53)
End of Phase 2	$R_{HA2-3} = \frac{2B_o}{W_P - B_o} + \frac{2B_o}{L_P - B_o} - \frac{4B_o^2}{(W_P - B_o)(L_P - B_o)}$ (21)
	$\hat{t}_{2-3} = 6\hat{t}_{1-2} = \frac{3\theta_{hydr} B_o^2}{k\Delta h}$ (46)
Phase 3	$R_{HA3} = \left( 2\sqrt{3B_o^2 + \frac{2k\hat{t}\Delta h}{\theta_{hydr}}} - 4B_o \right) \left( \frac{1}{W_P - B_o} + \frac{1}{L_P - B_o} \right) - \frac{\left[ 2\sqrt{3B_o^2 + (2k\hat{t}\Delta h/\theta_{hydr})} - 4B_o \right]^2}{(W_P - B_o)(L_P - B_o)}$ (55)
End of Phase 3	$R_{HAend} = 1.00 = 100\%$ (22)
	$\hat{t}_{end} = \frac{\theta_{hydr}}{8k\Delta h} (W_P^2 + 6W_P B_o - 3B_o^2) = \frac{\theta_{hydr}}{2k\Delta h} \left[ \left( \frac{W_P + B_o}{2} \right)^2 + B_o(W_P - B_o) \right]$ (47)

Note:  $\Delta h$  is given by Equation 2, 3 or 4; for bentonite hydration due to liquid migrating through geomembrane defects, use Equations 56 and 57.

$$R_{HA2} \approx C_{RHA} \frac{1}{W_P} \left( \sqrt{3B_o^2 + \frac{2k\hat{t}\Delta h}{\theta_{hydr}}} - B_o \right) \quad (65)$$

$$R_{HA2-3} \approx C_{RHA} \frac{2B_o}{W_P} \approx 2R_{HA1-2} \quad (66)$$

In the case of the third phase, a different dimensionless factor,  $C_{RHA3}$ , is used:

$$R_{HA3} \approx C_{RHA3} \frac{2}{W_P} \left( \sqrt{3B_o^2 + \frac{2k\hat{t}\Delta h}{\theta_{hydr}}} - 2B_o \right) \quad (67)$$

where

$$C_{RHAend} < C_{RHA3} < C_{RHA} \quad (68)$$

where  $C_{RHAend}$  is the value of the dimensionless factor at the end of Phase 3 (i.e. upon complete hydration of the bentonite layer).  $C_{RHA3}$  is close to  $C_{RHA}$  at the beginning of Phase 3 and close to  $C_{RHAend}$  at the end of Phase 3.

Equations 63 to 68 can also be found in Table 4. The dimensionless factor  $C_{RHA}$  depends on the geometric parameters of the panels ( $L_P$ ,  $W_P$  and  $B_o$ ). The dimensionless factor  $C_{RHAend}$  depends on  $W_P$  and  $B_o$ . A parametric study presented in Appendix 2 gives the values of  $C_{RHA}$  and  $C_{RHAend}$  that can be found in Table 5 for typical panel lengths and overlap widths. For practical purposes, the value of  $C_{RHA3}$  can be obtained by linear interpolation between  $C_{RHA}$  and  $C_{RHAend}$ .

The design examples presented in Section 4.2 will show that Equations 63 to 67 give an excellent approximation (1% or less in Phases 1 and 2) of the

rigorously calculated hydrated areas. The approximation in Phase 3 is generally not as good as in Phases 1 and 2, but is still acceptable in most cases.

#### 4.1.3. Assumptions

The main assumptions used to develop the equations presented in Tables 2 to 4 were presented at appropriate locations in this paper and are summarized below:

- The bentonite layer has a uniform thickness.
- The GM-GCL panels are joined by overlapping (overlap width  $B_o$ ).
- The geomembrane defects are assumed to be circular or can be approximately replaced by a circular defect with the same surface area.
- The size and frequency of geomembrane defects are assumed to be typical of geomembranes installed with good construction quality assurance practices (see Section 1.5 of the companion paper (Giroud and Daniel 2004)).
- The liquid is assumed to be water, or a liquid having properties similar to those of water.
- Diffusion of liquid through the geomembranes or the bentonite is not considered.
- No preferential path for liquid is considered between the bentonite layer and the geomembranes.

#### 4.1.4. Selection of parameter values

The values of relevant design parameters should be selected as follows:

- The thickness of the bentonite layer to be used in calculations is the thickness of the hydrated bentonite

**Table 4. Approximate equations for relative hydrated area and time for bentonite hydration due to water migration from the underlying soil through the GM-GCL panel overlaps**

Phase	Approximate equation for $B_o \ll W_p \ll L_p$
Phase 1	$R_{HA1} \approx C_{RHA} \frac{1}{W_p} \sqrt{\frac{2k\hat{t}\Delta h}{\theta_{hydr}}}$ (63)
End of Phase 1 (Interphase 1–2)	$R_{HA1-2} \approx C_{RHA} \frac{B_o}{W_p}$ (64)
Phase 2	$R_{HA2} \approx C_{RHA} \frac{1}{W_p} \left( \sqrt{3B_o^2 + \frac{2k\hat{t}\Delta h}{\theta_{hydr}}} - B_o \right)$ (65)
End of Phase 2 (Interphase 2–3)	$R_{HA2-3} \approx C_{RHA} \frac{2B_o}{W_p} \approx 2R_{HA1-2}$ (66)
Phase 3	$R_{HA3} \approx C_{RHA3} \frac{2}{W_p} \left( \sqrt{3B_o^2 + \frac{2k\hat{t}\Delta h}{\theta_{hydr}}} - 2B_o \right)$ (67)
	where: $C_{RHAend} < C_{RHA3} < C_{RHA}$ (68)

Note:  $\Delta h$  is given by Equation 2, 3 or 4;  $C_{RHA}$  and  $C_{RHAend}$  are given in Table 5;  $C_{RHA3}$  is to be interpolated between  $C_{RHA}$  and  $C_{RHAend}$ ; for bentonite hydration due to liquid migrating through the upper geomembrane, use Equations 56 and 57.

**Table 5. Values of the factors  $C_{RHA}$  and  $C_{RHAend}$  used in approximate equations for relative hydrated area and time for bentonite hydration due to water migration from the underlying soil through the GM-GCL panel overlaps (for  $W_p = 5.3$  m)**

Overlap width, $B_o$ (m)	Panel length, $L_p$ (m)	Factor $C_{RHA}$ (dimensionless)	Factor $C_{RHAend}$ (dimensionless)
0.15	60	1.11	1.03
	45	1.14	
	30	1.20	
	15	1.38	
0.30	60	1.14	1.06
	45	1.17	
	30	1.23	
	15	1.40	

layer under the overburden pressure expected in the field. Guidance is provided in Table 1. The initial thickness of the (unhydrated) bentonite layer is not a directly relevant parameter.

- The hydration volumetric content of the bentonite can be calculated as a function of the degree of saturation and thickness of the bentonite layer after hydration, using Equation A.12 or A.13 provided in Appendix 1. For GM-GCLs typically used in the United States, the values presented in Table 1 can be used.
- The hydraulic conductivity of the bentonite to be used in calculations is the hydraulic conductivity of saturated bentonite. This hydraulic conductivity should always be used (even if the hydrated bentonite is not saturated) when the recommended value of the suction head is used because the method was calibrated using the saturated hydraulic conductivity. The hydraulic conductivity of saturated bentonite depends on the overburden pressure. Guidance is provided in Table 1.
- The head difference that drives the migration of the hydration front should be determined as indicated in

Section 1.4. The recommended value of 3 m for the suction head at the hydration front should be used in conjunction with the saturated hydraulic conductivity for the hydraulic conductivity of the hydrated bentonite.

**4.2. Design examples**

Two examples are presented in this section: in Example 1, it is assumed that there is no defect in the geomembranes encapsulating the bentonite layer, and therefore all hydration is due to the overlaps; in Example 2, geomembrane defects are considered. Example 2 shows that, for typical conditions, the hydrated area due to liquid migrating through defects in the upper geomembrane can be neglected with respect to the hydrated area due to water migrating through the overlaps of the GM-GCL panels. The same conclusion would be reached for defects in the lower geomembrane.

**Example 1.** GM-GCL panels, overlapped at the edges, are overlain by a welded geomembrane and underlain by a coarse-grained soil. The liner system is subjected to an overburden pressure of 100 kPa. The GM-GCL panels

are 60 m long and 5.3 m wide, and they are overlapped by 0.15 m. The bentonite layer has a dry mass per unit area of approximately 4 kg/m<sup>2</sup> (0.8 lb/ft<sup>2</sup>). Calculate the time required to reach the end of each of the three phases of water migration. Also, calculate the relative hydrated area at 100 and 250 years after installation.

Since the dry mass per unit area of the bentonite layer is of the order of 3.9–4.4 kg/m<sup>2</sup> (0.8–0.9 lb/ft<sup>2</sup>), Table 1 can be used. The following values of the relevant parameters are obtained from Table 1 for an overburden pressure of 100 kPa:  $\theta_{hydr} = 0.40$  and  $k = 2 \times 10^{-11}$  m/s. According to Table 1, the thickness of the hydrated bentonite layer under 100 kPa is 6 mm; however, this information is not needed for the calculations presented hereafter.

As recommended in Section 1.4.4, a suction head of 3 m will be used for the bentonite. The underlying soil is coarse grained and thus the suction of the underlying soil is negligible. Therefore Equation 2 gives:

$$\Delta h = 3 - 0 = 3 \text{ m}$$

Equation 31 (Table 3) gives the time at the end of Phase 1 as follows:

$$\hat{t}_{1-2} = \frac{(0.40)(0.15)^2}{2(2 \times 10^{-11})(3)} = 75,000,000 \text{ s} = 2.4 \text{ years}$$

The relative hydrated area at the end of Phase 1 is given by Equation 20 (Table 3) as follows:

$$R_{HA1-2} = \frac{0.15}{5.3 - 0.15} + \frac{0.15}{60 - 0.15} - \frac{(0.15)^2}{(5.3 - 0.15)(60 - 0.15)} = 0.0315 = 3.15\%$$

Alternatively, the approximate Equation 64 (Table 4) can be used. The factor  $C_{RHA}$  in this equation is equal to 1.11 according to Table 5. Equation 64 gives:

$$R_{HA1-2} \approx 1.11 \times \frac{0.15}{5.3} \approx 0.0314 \approx 3.14\%$$

Note that, for this case, the approximation provided by Equation 64 is excellent (0.3% relative difference).

Equation 46 (Table 3) gives the time at the end of Phase 2 as follows:

$$\begin{aligned} \hat{t}_{2-3} &= 6\hat{t}_{1-2} = \frac{(3)(0.40)}{(2 \times 10^{-11})(3)}(0.15)^2 = 450,000,000 \text{ s} \\ &= 14.3 \text{ years} \end{aligned}$$

The relative hydrated area at the end of Phase 2 is given by Equation 21 (Table 3) as follows:

$$R_{HA2-3} = \frac{2 \times 0.15}{5.3 - 0.15} + \frac{2 \times 0.15}{60 - 0.15} - \frac{4(0.15)^2}{(5.3 - 0.15)(60 - 0.15)} = 0.0630 = 6.30\%$$

Alternatively, the approximate Equation 66 (Table 4) gives:

$$R_{HA2-3} \approx 1.11 \times \frac{2 \times 0.15}{5.3} = 0.0628 = 6.28\%$$

Note that, for this case, the approximation provided by Equation 66 is excellent (0.3% relative difference).

Equation 47 (Table 3) gives the time at the end of Phase 3 (i.e. the time for complete hydration) as follows:

$$\begin{aligned} \hat{t}_{end} &= \frac{0.40}{8(2 \times 10^{-11})(3)} [(5.3)^2 + 6(5.3)(0.15) - 3(0.15)^2] \\ &= 2.7327 \times 10^{10} \text{ s} = 866 \text{ years} \end{aligned}$$

Based on the above calculations, 100 and 250 years are in Phase 3. Therefore Equation 55 (Table 3) is to be used to calculate the relative hydrated area. Equation 55 is very long. For the sake of simplicity, the first term of Equation 55 is calculated first. This term is in fact the width of the hydrated area, according to Equation 54 (Table 2). The calculation for  $\hat{t} = 100$  years is as follows:

$$\begin{aligned} W_H &= 2\sqrt{3(0.15)^2 + \frac{2(2 \times 10^{-11})(100 \times 365 \times 86,400)(3)}{0.40}} \\ &\quad - 4(0.15) = 1.4135 \text{ m} \end{aligned}$$

Then Equation 55 gives

$$\begin{aligned} R_{HA100} &= \frac{1.4135}{5.3 - 0.15} + \frac{1.4135}{60 - 0.15} \\ &\quad - \frac{(1.4135)^2}{(5.3 - 0.15)(60 - 0.15)} = 0.2917 = 29.17\% \end{aligned}$$

Alternatively, the approximate Equation 67 (Table 4) can be used. To use Equation 67, it is necessary to select a value of the dimensionless factor  $C_{RHA3}$ . According to Equation 68 and Table 5,  $C_{RHA3}$  is between 1.03 for  $R_{HA} = 100\%$  (at the end of Phase 3) and 1.11 for  $R_{HA} = 6.3\%$  (the value calculated above for the beginning of Phase 3). Using 1.03 with the value 1.4135 calculated above, a first approximation of the hydrated area is calculated as follows:

$$R_{HA100} \approx 1.03 \left( \frac{1.4135}{5.3} \right) = 0.2747 = 27.47\%$$

Interpolating between  $C_{RHA} = 1.11$  for  $R_{HA} = 6.3\%$  and  $C_{RHAend} = 1.03$  for  $R_{HA} = 100\%$  gives

$$C_{RHA3} \approx 1.092 \text{ for } R_{HA} = 27.47\%$$

Hence:

$$R_{HA100} \approx 1.092 \times \frac{1.4135}{5.3} = 0.2912 = 29.12\%$$

Note that, for this case, the approximation provided by Equation 67 is excellent (0.2%).

Similar calculations for 250 years give:

$$W_H = 2.5194 \text{ m and } R_{HA250} = 51.07\%$$

**Example 2.** The same case as in Example 1 is considered; in addition, it is assumed that there may be 10 defects per hectare in the upper geomembrane, with an area of 1 cm<sup>2</sup> per defect. The maximum head of liquid on the upper

geomembrane during the design life of the liner is expected to be 0.3 m. Calculate the expected relative hydrated area 250 years after GCL installation.

First, the driving head is calculated using Equation 1 as follows:

$$\Delta h = 3 + 0.3 = 3.3 \text{ m}$$

Equation 56 gives:

$$\left[ \frac{4\pi(2 \times 10^{-11})(3.3)}{(0.4)(1 \times 10^{-4})} \right] (250 \times 365 \times 86,400) - 1 = \left( \frac{A_{Hdef}}{a} \right) \left[ \ln \left( \frac{A_{Hdef}}{a} \right) - 1 \right]$$

Hence:

$$163,469.89 = \left( \frac{A_{Hdef}}{a} \right) \left[ \ln \left( \frac{A_{Hdef}}{a} \right) - 1 \right]$$

Iterations give:

$$\frac{A_{Hdef}}{a} = 18,520.12$$

Hence, for an initial defect area, *a*, of 1 cm<sup>2</sup>:

$$A_{Hdef} = (18,520.12)(1 \times 10^{-4}) = 1.852 \text{ m}^2$$

As the defect is circular, the hydrated area will be circular, and the radius of the hydrated area is:

$$R = \sqrt{\frac{1.852}{\pi}} = 0.77 \text{ m}$$

For a ‘typical’ value for ‘good’ construction quality assurance of 10 defects per hectare, the relative hydrated area due to leakage through geomembrane defects is given by Equation 57 as follows:

$$R_{HAdef} = \frac{(10)(1.852)}{10,000} = 0.0019 \approx 0.2\%$$

This value of 0.2% is negligible compared with the value of 51% calculated in Example 1 for the relative hydrated area due to water migrating from the underlying soil through the GM-GCL panel overlaps. It should be noted that the calculation performed above is conservative (i.e. it gives an upper boundary for the hydrated area) because the maximum head was used. A smaller value of the hydrated area would have been obtained with an average value of the head.

## 5. INFLUENCE OF PARAMETERS

### 5.1. Overview of the parameters

Based on the equations for the relative hydrated area presented in Table 3, the rate at which a bentonite layer encapsulated between two geomembranes becomes hydrated depends on the following parameters: the length, *L<sub>P</sub>*, and width, *W<sub>P</sub>*, of the panels; the overlap width, *B<sub>o</sub>*; the hydration volumetric content, *θ<sub>hydr</sub>*, and the hydraulic conductivity, *k*, of the bentonite; and the suction heads in the bentonite and the underlying soil that govern the head difference, *Δh*.

These parameters were defined and discussed in the following sections: panel geometry (*L<sub>P</sub>*, *W<sub>P</sub>*, and *B<sub>o</sub>*) in Section 1.1; hydration volumetric content in Section 1.5.2; hydraulic conductivity in Section 1.5.3; and suction in Section 1.4. Their influence on bentonite layer hydration is discussed in the subsequent sections.

### 5.2. Influence of hydraulic conductivity

The bentonite hydraulic conductivity, *k*, has a large influence on the rate of hydration. Equations 30, 31, 45, 46 and 47 show that the time required for the hydration front to reach a certain distance (and hence the time required to reach any given relative hydrated area, such as 50%) is inversely proportional to *k*. Thus hydration is 50 times faster in the case representative of a landfill cover (*k* = 5 × 10<sup>-11</sup> m/s under 10 kPa) than in the case representative of a landfill liner (*k* = 1 × 10<sup>-12</sup> m/s under 500 kPa, which corresponds to approximately 40 m of waste) because the bentonite hydraulic conductivity is 50 times greater under a 10 kPa overburden pressure than under a 500 kPa overburden pressure. This is illustrated in Table 6, which gives the time required for hydration of the entire bentonite panel in the case of representative liner and cover situations for the following values of the parameters: overlap width, *B<sub>o</sub>* = 0.15 m; panel width, *W<sub>P</sub>* = 5.2 m; panel length, *L<sub>P</sub>* = 61 m; and hydration volumetric content, *θ<sub>hydr</sub>* = 0.4.

### 5.3. Influence of suction

The head difference, *Δh*, that drives bentonite hydration has a significant impact on the rate of hydration. Equations 30, 31, 45, 46 and 47 show that the time required for the hydration front to reach a certain distance (and hence the time required to reach any given relative hydrated area, such as 50%) is inversely proportional to *Δh*. As indicated by Equation 2, an

**Table 6. Time required for hydrating the entire panel (for *θ<sub>hydr</sub>* = 0.40, *L<sub>P</sub>* = 61 m, *W<sub>P</sub>* = 5.2 m, and *B<sub>o</sub>* = 0.15 m)**

Bentonite hydraulic conductivity	<i>s<sub>b</sub></i> = 3 m		<i>s<sub>b</sub></i> = 10 m	
	<i>s<sub>s</sub></i> = 1 m <i>Δh</i> = 2 m	<i>s<sub>s</sub></i> = 0 m <i>Δh</i> = 3 m	<i>s<sub>s</sub></i> = 1 m <i>Δh</i> = 9 m	<i>s<sub>s</sub></i> = 0 m <i>Δh</i> = 10 m
1 × 10 <sup>-12</sup> m/s	25,000 yrs	17,000 yrs	5500 yrs	5000 yrs
5 × 10 <sup>-11</sup> m/s	500 yrs	330 yrs	110 yrs	100 yrs

important part of the head difference (especially in the case of landfills) is due to the suction head in the bentonite at the hydration front. Therefore the assumed value of the bentonite suction head at the hydration front has a significant impact on the calculated value of the time required for hydration. This is illustrated in Table 6, which gives the time required for hydration of the entire bentonite panel for the following values of the parameters: overlap width,  $B_o = 0.15$  m; panel width,  $W_p = 5.2$  m; panel length,  $L_p = 61$  m; and hydration volumetric content,  $\theta_{\text{hydr}} = 0.4$ . In Table 6, two values of the suction head in the bentonite at the hydration front are used:  $s_b = 3$  m, as recommended in Section 1.4.4, and  $s_b = 10$  m, to evaluate the impact of the more conservative assumption of a greater suction head (i.e. an assumption leading to a faster calculated hydration).

In contrast, the range of values used in Table 6 for the suction head in the underlying soil,  $s_s$ , is too narrow (0 to 1 m) to have a marked influence on the hydrated area if the suction head in the bentonite at the hydration front,  $s_b$ , is equal to or greater than 3 m. This narrow range of values of soil suction head was used in Table 3 because soil suction head typically varies between 0 m (coarse-grained soils or saturated fine-grained soils) and 1 m (dry fine-grained soils), as discussed in Section 1.4.4. While a suction head of greater than 1 m is possible in some fine-grained natural soils (e.g. high-plasticity clay), capping the suction head of the underlying soil at 1 m is a conservative assumption (i.e. it increases the calculated hydration rate and hydrated area).

#### 5.4. Combined influence of hydraulic conductivity and head difference

All of the equations that contain  $\Delta h$  (the head difference) also contain  $k$  (the hydraulic conductivity of the bentonite). Furthermore, in all these equations, these two parameters appear as the product,  $k\Delta h$ . Therefore the same relative hydrated area is obtained for various sets of values of  $k$  and  $\Delta h$  that are such that the product  $k\Delta h$  is constant.

The recommended suction head at the hydration front of 3 m is based upon back-analyses of observed moisture migration (Giroud and Daniel 2004). To perform these back-analyses, a hydraulic conductivity had to be assumed for the hydrated bentonite because the actual hydraulic conductivity of the hydrated bentonite was not known. A relatively high value was used for the hydraulic conductivity (i.e. a value equal, or almost equal, to the saturated hydraulic conductivity). If the actual value of the hydraulic conductivity had been known and used, and if that value was significantly less than the saturated hydraulic conductivity, a value greater than 3 m would have been back-calculated for the suction head at the hydration front. This consideration does not affect numerical calculations performed using the methodology presented in this paper if the assumptions are similar to those made in the back-analyses (in particular if a hydration front suction of 3 m is used in conjunction with the saturated hydraulic

conductivity for the hydraulic conductivity of the hydrated bentonite, as recommended in Section 1.4.4).

Even though numerical calculations are not affected by the respective values of  $k$  and  $\Delta h$  as long as the  $k\Delta h$  product is correct, the phenomenon of water migration would be better understood if  $k$  and  $\Delta h$  were known independently. Accordingly, experimental research to develop a better knowledge of the bentonite suction head at the hydration front and the hydraulic conductivity of the hydrated bentonite is recommended, considering the importance of these two parameters.

#### 5.5. Influence of hydration volumetric content

The hydration volumetric content of the bentonite has a large influence on the rate of hydration. Equations 30, 31, 45, 46 and 47 show that the time required for the hydration front to reach a certain distance (hence the time required to reach any given relative hydrated area, such as 50%) is proportional to  $\theta_{\text{hydr}}$ . Therefore it is conservative to perform calculations with a low value of the hydration volumetric content, which gives short hydration times or, for a given time, a large hydrated area. As shown in the study presented in Appendix 1, the hydration volumetric content is a function of the assumed degree of saturation of the hydrated bentonite. A degree of saturation of 0.8–0.9 was used to obtain the hydration volumetric content values proposed in Table 1. More conservative designs could be done by assuming a smaller value of the degree of saturation. Experimental research is recommended to develop a better knowledge of the degree of saturation of hydrated bentonite in GCLs.

#### 5.6. Influence of overlap width

Nominal overlaps between 0.15 m and 0.3 m are typically used in the field in the United States with GM-GCL panels. Figure 9 illustrates the influence of the overlap width (0.15 m and 0.3 m) for the case of a landfill liner (i.e. bentonite hydraulic conductivity of  $1 \times 10^{-12}$  m/s, which corresponds to an overburden pressure of 500 kPa, according to Table 1), with a head difference of 3 m and a hydration volumetric content of 0.4. In Figure 9, the panel width is 5.1 m and the panel length is 61 m. It appears in Figure 9 that the impact of overlap width on hydrated area does not follow a simple pattern. To interpret Figure 9, it is useful to calculate the transition times using Equations 31 and 46. The following values are obtained for the 0.15 m overlap (dashed curve in Figure 9):

$$\hat{t}_{1-2} = 48 \text{ years and } \hat{t}_{2-3} = 285 \text{ years}$$

and the following values for the 0.3 m overlap (solid curve in Figure 9):

$$\hat{t}_{1-2} = 190 \text{ years and } \hat{t}_{2-3} = 1142 \text{ years}$$

For the first 48 years, the 0.15 m wide overlap and the 0.3 m wide overlap correspond approximately to the same hydrated area (the relative hydrated area at 48 years is 3.3% with the 0.15 m wide overlap and 3.4% with the 0.3 m wide overlap). Then, between 48 years

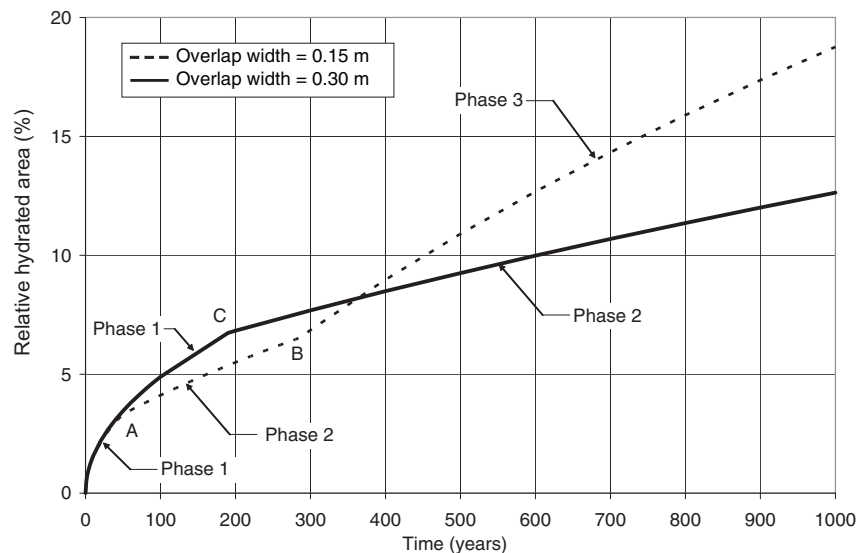


Figure 9. Influence of overlap width on hydrated area (for  $\theta_{\text{hydr}} = 0.4$ ,  $k = 1 \times 10^{-12}$  m/s,  $\Delta h = 3$  m,  $L_P = 61$  m and  $W_P = 5.1$  m)

and 360 years, a larger hydrated area is achieved with the 0.3 m wide overlap than with the 0.15 m wide overlap. Finally, beyond 360 years, a larger hydrated area is achieved with the 0.15 m wide overlap than with the 0.3 m wide overlap. This complex pattern is due to the three different phases of hydration of the encapsulated bentonite:

- During Phase 1, when the overlap is becoming hydrated, the rate of hydration is at its quickest because the thickness of bentonite available for flow is the smallest, and is independent of the overlap width. However, the duration of Phase 1 depends on the overlap width.
- During Phase 2, the rate of hydration decreases because the flow bifurcates and the thickness of bentonite available for flow doubles. During Phase 2, the 'virgin' hydration front advances in only one direction because, in the other direction, the hydration front is 'doubling back' (Figures 6b and 7b) over the already-hydrated overlap.
- During Phase 3, the rate of bentonite hydration increases because the hydration front that doubled back has advanced beyond the leading edge of the overlap, and the virgin hydration front is advancing on both sides of the overlap.

These three phases of encapsulated bentonite hydration are delineated by the following points in Figure 9: A (48 years), B (285 years) and C (190 years). These points correspond to the values of  $\hat{t}_{1-2}$  and  $\hat{t}_{2-3}$  given above. The point for 1142 years (i.e.  $\hat{t}_{2-3}$  for the 0.3 m overlap) would be beyond the frame of Figure 9.

Figure 9 shows that the time required to reach a relative hydrated area of 12% is 60% greater with an overlap width of 0.3 m than with an overlap of 0.15 m. This difference is large because, in this case, hydration is in Phase 2 with the 0.3 m overlap and in Phase 3 with the 0.15 m overlap. The difference is smaller (i.e. 14%) at 100% hydration, as shown by using Equation 47, which

gives 16,136 years for  $B_o = 0.15$  m and 18,455 years for  $B_o = 0.3$  m.

### 5.7. Influence of panel length

GCL panels are typically provided in rolls 30 to 60 m long in the United States. GCL rolls that are 60 m long are heavy and, for this reason, 30 m long rolls are often preferred on slopes. The influence of panel length is more marked at the beginning of the hydration process than at the end. In fact, Equation 47 shows that, as long as the panel length is greater than its width, the time required for complete hydration is independent of panel length (which results from the assumption of 'right-angle corners' made in Section 2.1). The influence of panel length in Phases 1 and 2 can be quantified using the parametric study (presented in Appendix 2) that led to the values of the dimensionless factor  $C_{\text{RHA}}$  presented in Table 5. By dividing the  $C_{\text{RHA}}$  values for panel lengths of 45 m, 30 m and 15 m by the value for 60 m, it appears that the hydrated area for a panel length of 60 m should be multiplied by the following factors: 1.03 if the panel length is 45 m, 1.08 if the panel length is 30 m, and 1.23 if the panel length is 15 m. These factors are valid only for Phases 1 and 2; they decrease progressively to 1.00 as hydration progresses in Phase 3. It may be concluded that the influence of panel length on the extent of the hydrated area is less marked than the influence of the other parameters.

## 6. IMPACT OF HYDRATED AREA ON INTERFACE SHEAR STRENGTH

### 6.1. General considerations concerning GCL shear strength

Advantages with respect to liquid containment capability notwithstanding, another motivation (sometimes the primary motivation) for encapsulating a GM-GCL in practice is mitigation of the strength loss associated with bentonite hydration due to water migrating from the

underlying soil. The low shear strength of saturated bentonite is well recognized in geotechnical practice (e.g. Stark and Eid 1994). Some of the most dramatic failures in geotechnical engineering have been attributed to saturated bentonite layers (e.g. Watry and Lade 2000). Testing by Daniel (1993) indicates that the shear strength of bentonite hydrated to a moisture content of 50% approaches the shear strength of saturated bentonite for normal stress of 150 kPa or less. Therefore it is assumed herein that the shear strength of the hydrated portion of an encapsulated GM-GCL is equal to the shear strength of saturated bentonite. Errors introduced by this assumption are conservative with respect to shear strength and stability, as the saturated shear strength is the lowest possible shear strength of bentonite for a given normal stress. It is further assumed that the shear strength of the bentonite at the factory moisture content is representative of the unhydrated, or 'dry', portion of an encapsulated GM-GCL.

Bentonite exhibits a stress-strain behavior characterized by a peak and a residual shear strength under both dry and saturated conditions. The choice of which shear strength (peak or residual) to use is up to the design engineer, and may be related to the design factor of safety and mode and consequences of failure. Residual shear strength is often associated with a lower acceptable factor of safety than peak shear strength (Sabatini *et al.* 2001, 2002). Residual shear strength is typically used for 'pre-sheared' surfaces and for 'Newmark'-type seismic deformation calculations (Kavazanjian 1999). Use of residual shear strength is intended to preclude the potential for progressive failure due to post-peak strength decrease, as progressive failure occurs when the factor of safety is greater than 1.0 using a peak (or pre-residual) strength but is less than 1.0 with the residual strength. Thiel *et al.* (2001) recommend the use of residual shear strength and a factor of safety greater than 1.0 combined with the assumption of 100% relative hydrated area as a supplementary stability criterion for encapsulated GM-GCL systems employed in critical environmental applications (e.g. landfill base liner stability).

## 6.2. Shear strength of bentonite

Although project-specific testing is the most accurate means of assessing the shear strength of 'dry' and hydrated bentonite in an encapsulated GM-GCL application, representative values from previous laboratory testing programmes on commercially available GM-GCLs may also be used. The equations presented hereafter (i.e. Equations 69 to 76) give the shear strength of a specific GM-GCL available in the United States. These equations were developed based on data presented by Thiel *et al.* (2001). The parameters in the equations are:  $\tau$  = consolidated drained shear strength; and  $\sigma$  = normal (consolidation) stress.

The following equations are for the peak and residual consolidated drained shear strength of 'dry' (unhydrated) bentonite (moisture content less than 30%) for the specific GM-GCL mentioned above:

$$\tau_{\text{peak-dry}} = \sigma \tan 48^\circ \text{ for } \sigma \leq 100 \text{ kPa} \quad (69)$$

$$\tau_{\text{peak-dry}} = 160 \left\{ 1 - \frac{1}{[1 + (\sigma/500)]^{3.6}} \right\} + 0.34 \sigma \quad (70)$$

for  $\sigma \geq 100 \text{ kPa}$

$$\tau_{\text{residual-dry}} = \sigma \tan 42^\circ \text{ for } \sigma \leq 100 \text{ kPa} \quad (71)$$

$$\tau_{\text{residual-dry}} = 100 \left\{ 1 - \frac{1}{[1 + (\sigma/400)]^{4.6}} \right\} + 0.26 \sigma \quad (72)$$

for  $\sigma \geq 100 \text{ kPa}$

where:  $\tau_{\text{peak-dry}}$  = peak shear strength of dry bentonite; and  $\tau_{\text{residual-dry}}$  = residual shear strength of dry bentonite. Note that Equations 70 and 72 are unit-specific: the normal stress must be given in kPa.

The shear strength of saturated (hydrated) bentonite is typically presented as a consolidated drained strength envelope. However, it should be kept in mind that the strength given by this envelope represents the undrained strength of the bentonite consolidated under the given normal stress: changes in normal stress during shear (e.g. normal stress redistribution) will not affect the strength of saturated bentonite, as the bentonite does not have time to consolidate under the change in stress. For the specific GM-GCL mentioned above, the equations for the peak and residual shear strength of hydrated GM-GCL are:

$$\tau_{\text{peak-hydr}} = 10 \left\{ 1 - \frac{1}{[1 + (\sigma/150)]^{3.8}} \right\} + 0.12 \sigma \quad (73)$$

for  $\sigma \leq 150 \text{ kPa}$

$$\tau_{\text{peak-hydr}} = 45 \left\{ 1 - \frac{1}{[1 + (\sigma/1800)]^8} \right\} + 0.04 \sigma \quad (74)$$

for  $\sigma \geq 150 \text{ kPa}$

$$\tau_{\text{residual-hydr}} = \sigma \tan 8^\circ \text{ for } \sigma \leq 150 \text{ kPa} \quad (75)$$

$$\tau_{\text{residual-hydr}} = 37 \left\{ 1 - \frac{1}{[1 + (\sigma/1800)]^{6.5}} \right\} + 0.04 \sigma \quad (76)$$

for  $\sigma \geq 150 \text{ kPa}$

where:  $\tau_{\text{peak-hydr}}$  = peak shear strength of hydrated bentonite; and  $\tau_{\text{residual-hydr}}$  = residual shear strength of hydrated bentonite. Note that Equations 73, 74 and 76 are unit-specific, requiring the use of normal stress in kPa, and assume the normal load is applied prior to hydration.

## 6.3. Prorated shear strength for encapsulated GM-GCL design

The internal shear strength of an encapsulated GM-GCL may be evaluated as a function of the relative hydrated area and the shear strength of the hydrated and 'dry' (unhydrated) bentonite. This internal shear strength must be compared with the interface shear strength of the encapsulating geomembranes with the overlying and underlying soil to determine the governing shear strength for stability assessment. The internal shear strength of the encapsulated GM-GCL, referred to herein as the 'prorated shear strength', may be calculated as:

$$\tau_{\text{prorated}} = \tau_{\text{dry}} - R_{\text{HA}}(\tau_{\text{dry}} - \tau_{\text{hydr}}) \quad (77)$$

**Table 7. Prorated shear strength as a function of the relative hydrated area (for the specific GM-GCL mentioned in Section 6.2)**

Relative hydrated area (%)	$\sigma = 10 \text{ kPa}$		$\sigma = 500 \text{ kPa}$	
	Peak shear strength (kPa)	Residual shear strength (kPa)	Peak shear strength (kPa)	Residual shear strength (kPa)
100	3.4	1.4	58.7	49.5
80	4.9	2.9	110.3	85.1
60	6.5	4.4	161.9	120.7
40	8.0	6.0	213.6	156.4
20	9.6	7.5	265.2	192.0
0	11.1	9.0	316.8	227.6

where:  $\tau_{\text{prorated}}$  = prorated shear strength;  $\tau_{\text{dry}}$  = shear strength of dry bentonite; and  $\tau_{\text{hydr}}$  = shear strength of hydrated bentonite. The relative hydrated area,  $R_{\text{HA}}$ , is calculated using the equations summarized in Section 4.1, and the relevant values for shear strength of dry and hydrated bentonite may be calculated using Equations 69 to 76, as appropriate, if the specific GM-GCL mentioned in Section 6.2 is used.

As indicated by Equation 77 (when combined with Equations 69 to 76, as appropriate), the prorated shear strength of an encapsulated GM-GCL depends upon the relative hydrated area and the applied normal stress. Table 7 illustrates the impact of these factors on both peak and residual shear strength for applied normal stresses of 10 kPa (representative of a typical landfill cover) and 500 kPa (representative of a landfill liner with approximately 40 m of waste overburden) in the case of the specific GM-GCL mentioned in Section 6.2. Table 7 illustrates the benefit, with respect to shear strength and stability, provided by minimizing the relative hydrated area through the use of an encapsulated GM-GCL.

## 7. CONCLUSIONS

The analyses presented in this paper are based on generally accepted assumptions (such as the Green-Ampt assumption), and were calibrated using a limited amount of laboratory and field data. More experimental work to validate and calibrate the model is recommended, as noted below. Also, additional analytical work to evaluate liquid and vapor migration due to diffusion through geomembranes and bentonite may be warranted. In spite of the limitations resulting from the assumptions and the mechanisms considered, the analyses presented in this paper lead to a methodology that can be used by practicing engineers for liner design.

The equations presented in this paper make it possible to evaluate the area of hydrated bentonite, and thus the shear strength, in the case of overlapped GM-GCL panels overlain by a welded geomembrane. Two hydration mechanisms were considered: hydration by water from the underlying soil migrating through overlaps of

the GM-GCL panels, and hydration by liquid migrating through geomembrane defects. Numerical calculations show that, based upon the assumptions and recommended parameter values described herein, the second mechanism is negligible for typical landfill applications.

The main parameters that govern the hydrated area due to water migration through the overlaps of GM-GCL panels in the equations developed herein are: the saturated hydraulic conductivity of the bentonite, the head difference that drives the migration of water, the amount of water required to hydrate the bentonite (expressed by the hydration volumetric content), the overlap width, and the panel length. Numerical calculations performed to evaluate the influence of these parameters on the extent of the hydrated area for a given time (or the time required to reach a certain relative hydrated area) showed the following:

- The influence of the bentonite saturated hydraulic conductivity, which depends significantly on overburden pressure, on the extent of the hydrated area is very large. Therefore there is a large difference between the hydration rate for landfill covers (low overburden pressure) and that for landfill liners (high overburden pressure). The use of the saturated hydraulic conductivity is linked to the recommended value of 3 m for the suction head in the bentonite at the hydration front, as the analyses used by Giroud and Daniel (2004) to establish this suction head value were calibrated based upon hydration front migration rates observed in field and laboratory tests and interpreted using the saturated hydraulic conductivity of the bentonite. More experimental research is needed on the degree of saturation of hydrated bentonite and the hydraulic conductivity of unsaturated bentonite.
- The influence of suction in the bentonite at the hydration front on the extent of the hydrated area is large because the hydrated area increases significantly for increasing values of the head difference (which is generally governed by suction at the hydration front). There is some uncertainty with respect to this parameter, as little information is available on the

magnitude of bentonite suction at the hydration front. More experimental research is recommended in this area.

- The amount of water required to hydrate the bentonite is quantified by the 'hydration volumetric content'. More experimental research is needed on the value of this parameter. Guidance for assuming a value for the hydration volumetric content is provided in this paper, based on a parametric study.
- The influence of the overlap width is complex. Increasing the width of the overlaps of the GM-GCL panels increases the rate at which the relative hydrated area increases over short time periods and decreases this rate for longer time periods. However, if only typical overlaps used in the field are considered, the influence of overlap width is small compared with the influence of other parameters such as the bentonite hydraulic conductivity and the bentonite suction at the hydration front.
- The influence of panel length on the extent of the hydrated area is less marked than the influence of the other parameters.

Considering the significant influence of some parameters on the extent of the hydrated area, it is important to select the parameter values used in design properly and conservatively. Information provided in this paper can be used as design guidance.

## ACKNOWLEDGEMENTS

This paper is an expanded version of a previously published paper (Giroud *et al.* 2002). The previously published paper did not include an evaluation of the hydrated area due to liquid migrating through geomembrane defects, nor a complete set of practical equations for design, and did not address the calculation of the shear strength as a function of the relative hydrated area. Furthermore, the previously published paper contained some errors, as indicated in Appendix 3.

Part of this work was developed during the preparation of a GCL design manual. The support of GSE and the leadership of R. B. Erickson for the preparation of the manual are acknowledged.

The support of GeoSyntec Consultants is acknowledged. Finally, the authors are grateful to D. E. Daniel for many valuable discussions, and to F. J. Lauro, who contributed to the previously published paper.

## APPENDIX 1. HYDRATION VOLUMETRIC CONTENT

Prior to the beginning of hydration, the bentonite layer is characterized by the following parameters:  $t_0$  = initial thickness of the bentonite layer;  $w_0$  = initial moisture content of the bentonite; and  $\mu_0$  = initial mass per unit area of the bentonite layer. After hydration, the bentonite layer is characterized by the following parameters:  $t_h$  = thickness of the hydrated bentonite layer;  $w_h$  = moisture content of the hydrated bentonite; and

$\mu_h$  = mass per unit area of the hydrated bentonite layer. The terminology 'moisture content' with the symbol  $w$  is used for the moisture content by mass, whereas the symbol  $\theta$  will be used for the moisture content by volume (volumetric moisture content). The following classical relationship exists between  $w$  and  $\theta$ :

$$\theta = w(1 - n) \frac{\rho_s}{\rho_w} \quad (\text{A.1})$$

where:  $\theta$  = volumetric moisture content of the bentonite;  $w$  = moisture content of the bentonite;  $n$  = porosity of the bentonite;  $\rho_s$  = density of the bentonite particles; and  $\rho_w$  = density of water.

It should be noted that both  $\mu_0$  and  $\mu_h$  include the mass of bentonite and the mass of water present in the bentonite layer. The following classical relationship exists:

$$\frac{\mu_0}{1 + w_0} = \frac{\mu_h}{1 + w_h} = \mu_d \quad (\text{A.2})$$

where  $\mu_d$  is the dry mass per unit area of the bentonite layer (i.e. the mass per unit area of the dry bentonite layer, which is the bentonite layer with zero moisture content). The dry mass per unit area remains constant as the moisture of the bentonite changes owing to swelling or compression associated with hydration and overburden pressure. Two variables, the porosity of the bentonite and the thickness of the bentonite layer, are linked to the dry mass per unit area by the following classical relationship:

$$n = 1 - \frac{\mu_d}{\rho_s t} \quad (\text{A.3})$$

where  $t$  is the thickness of the bentonite layer. When the thickness changes (swelling or compression), the porosity changes in accordance with Equation A.3, while the dry mass per unit area remains constant.

The amount of water added to the bentonite layer between the initial state and the hydrated state is characterized by the mass per unit area of water added for hydration,  $\mu_w$ , which is given by the following equation:

$$\mu_w = \mu_h - \mu_0 \quad (\text{A.4})$$

This mass of water per unit area is the mass of a volume of water that occupies a unit area and has a thickness equal to

$$t_w = \frac{\mu_w}{\rho_w} \quad (\text{A.5})$$

where:  $t_w$  = equivalent thickness of the water added for hydration.

The hydration volumetric content is defined as the ratio between: (i) the volume of water added to the bentonite between the initial state and the hydrated state; and (ii) the total volume of the hydrated bentonite. The volume ratio is equal to the thickness ratio:

$$\theta_{\text{hydr}} = \frac{t_w}{t_h} \quad (\text{A.6})$$

where:  $\theta_{\text{hydr}}$  = hydration volumetric content. It is important to note that the hydration volumetric content is generally not the difference between volumetric moisture content in the hydrated bentonite and the initial volumetric moisture content of the bentonite because the volume of the bentonite generally changes between the initial state and the hydrated state.

Combining Equations A.4 to A.6 gives:

$$\theta_{\text{hydr}} = \frac{\mu_d(w_h - w_0)}{\rho_w t_h} \quad (\text{A.7})$$

Equation A.7 makes it possible to calculate the hydration volumetric content if the moisture content of the hydrated bentonite is known. This may be the case in a laboratory or a field test. However, at the design stage, the moisture content of the hydrated bentonite is not known. Therefore an assumption must be made. Instead of making an assumption on the moisture content, it is more convenient to make an assumption on the degree of saturation of the hydrated bentonite, as explained below.

At the design stage, although the moisture content of the hydrated bentonite is not known, its upper limit is known. The upper limit of the moisture content is reached when the bentonite is saturated (i.e. when the entire pore space is occupied by water). The volumetric moisture content,  $\theta$ , is then equal to the porosity,  $n$ . Hence from Equation A.1:

$$w_{\text{sath}} = \left( \frac{n}{1-n} \right) \frac{\rho_w}{\rho_s} \quad (\text{A.8})$$

where  $w_{\text{sath}}$  is the saturated moisture content of the hydrated bentonite (i.e. the moisture content that the hydrated bentonite would have if it were saturated without volume change between the hydrated state and the saturated state). Combining Equations A.3 and A.8 gives

$$w_{\text{sath}} = \frac{\rho_w t_h}{\mu_d} - \frac{\rho_w}{\rho_s} \quad (\text{A.9})$$

The following classical relationship exists between the hydrated moisture content and the saturated moisture content:

$$w_h = S_h w_{\text{sath}} \quad (\text{A.10})$$

where:  $S_h$  = degree of saturation of the bentonite in the hydrated state ( $0 \leq S_h \leq 1.0$ ).

Combining Equations A.8 and A.10 gives:

$$w_h = S_h \left( \frac{\rho_w t_h}{\mu_d} - \frac{\rho_w}{\rho_s} \right) \quad (\text{A.11})$$

Combining Equations A.7 and A.11 gives:

$$\theta_{\text{hydr}} = S_h - \frac{\mu_d}{\rho_w t_h} \left( \frac{S_h}{\rho_s / \rho_w} + w_0 \right) \quad (\text{A.12})$$

Equation A.12 gives the hydration volumetric content of the bentonite layer for an assumed value of the degree of saturation of the hydrated bentonite,  $S_h$ , and for values of two characteristics of the hydrated bentonite layer that should be known: the thickness of the hydrated bentonite layer,  $t_h$ , and the dry mass per unit area of the

bentonite layer,  $\mu_d$ . The initial moisture content of the bentonite,  $w_0$ , is assumed to be known, and the values of  $\rho_w$  and  $\rho_s$  are not variable.

There are many cases where it is not convenient to use the dry mass per unit area of the bentonite layer in design calculations. These are cases where the specified value is not the dry mass per unit area of the bentonite,  $\mu_d$ , but the mass per unit area including the water present in the bentonite before hydration,  $\mu_0$ . In those cases, it is preferable to use the following equation, obtained by combining Equations A.2 and A.12:

$$\theta_{\text{hydr}} = S_h - \frac{\mu_0}{(1+w_0)\rho_w t_h} \left( \frac{S_h}{\rho_s / \rho_w} + w_0 \right) \quad (\text{A.13})$$

Hydration of a bentonite layer may result in swelling of the bentonite if the overburden stress is small or compression of the bentonite if the overburden stress is large. Swelling results in a thickness increase of the bentonite layer, and compression results in a thickness decrease of the bentonite layer.

Under a high overburden pressure, it may happen that the extent of the compression is such that the amount of water expelled owing to bentonite compression is greater than the amount of water needed to hydrate the bentonite, which results in a negative hydration volumetric content. It is useful to quantify the case of zero hydration volumetric content, which provides a limit of applicability of Equations A.12 and A.13. The case of zero hydration volumetric content can be quantified by writing that  $w_{\text{sath}}$  from Equation A.9 is equal to  $w_0/S_h$  or by writing  $\theta_{\text{hydr}} = 0$  in Equation A.12 or A.13. Hence, after simplifications:

$$t_{\text{hlim}} = \mu_d \left( \frac{1}{\rho_s} + \frac{w_0}{S_h} \right) = \frac{\mu_0}{1+w_0} \left( \frac{1}{\rho_s} + \frac{w_0}{S_h} \right) \quad (\text{A.14})$$

where:  $t_{\text{hlim}}$  = limit value of the hydrated bentonite layer thickness below which the hydration volumetric content is negative.

Values of the hydration volumetric content as a function of the hydrated bentonite layer thickness and the bentonite degree of saturation are presented in three tables in order to evaluate the influence the various parameters: Table A.1 for a dry mass per unit area of bentonite of 3.66 kg/m<sup>2</sup> (0.75 lb/ft<sup>2</sup>) and an initial moisture content of 25%; Table A.2 for an initial moist mass per unit area of bentonite of 4.9 kg/m<sup>2</sup> (1.0 lb/ft<sup>2</sup>) and an initial moisture content of 25%; and Table A.3 for an initial moist mass per unit area of bentonite of 4.9 kg/m<sup>2</sup> (1.0 lb/ft<sup>2</sup>) and an initial moisture content of 15%. In all three tables, the density of bentonite particles was assumed to be 2700 kg/m<sup>3</sup> (i.e. a specific gravity of the bentonite particles of 2.7). The limit values of the hydrated bentonite layer thickness in Tables A.1 to A.3 were calculated using Equation A.14.

The maximum possible value of the volumetric moisture content of a soil is the porosity of this soil. Therefore it is interesting to complete Tables A.1 to A.3 by calculating the porosity of the bentonite in the hydrated state. The porosity of the hydrated bentonite is

**Table A.1. Hydration volumetric content and porosity of hydrated bentonite as a function of the thickness of the hydrated bentonite layer and the degree of saturation of the bentonite (for  $w_0 = 25\%$ ,  $\mu_d = 3.66 \text{ kg/m}^2 = 0.75 \text{ lb/ft}^2$ , and  $\rho_s = 2700 \text{ kg/m}^3$ )**

Thickness of hydrated bentonite layer, $t_h$	Hydration volumetric content of hydrated bentonite, $\theta_{hydr}$				Porosity of hydrated bentonite, $n_h$
	Degree of saturation of hydrated bentonite, $S_h$				
	0.7	0.8	0.9	1.0	
2 mm	< 0	< 0	< 0	< 0	0.32
$t_{hlim} = 2.27 \text{ mm}$ for $S_h = 1.0$	< 0	< 0	< 0	0.00	0.40
$t_{hlim} = 2.37 \text{ mm}$ for $S_h = 0.9$	< 0	< 0	0.00	0.04	0.43
$t_{hlim} = 2.50 \text{ mm}$ for $S_h = 0.8$	< 0	0.00	0.05	0.09	0.46
$t_{hlim} = 2.66 \text{ mm}$ for $S_h = 0.7$	0.00	0.05	0.10	0.15	0.49
3 mm	0.08	0.13	0.19	0.24	0.55
4 mm	0.23	0.30	0.37	0.43	0.66
5 mm	0.33	0.40	0.47	0.55	0.73
6 mm	0.39	0.47	0.54	0.62	0.77
7 mm	0.43	0.51	0.59	0.68	0.81
8 mm	0.47	0.55	0.63	0.72	0.83
9 mm	0.49	0.58	0.66	0.75	0.85

**Table A.2. Hydration volumetric content and porosity of hydrated bentonite as a function of the thickness of the hydrated bentonite layer and the degree of saturation of the bentonite (for  $w_0 = 25\%$ ,  $\mu_0 = 4.9 \text{ kg/m}^2 = 1 \text{ lb/ft}^2$  (i.e.  $\mu_d = 3.9 \text{ kg/m}^3 = 0.8 \text{ lb/ft}^2$ ), and  $\rho_s = 2700 \text{ kg/m}^3$ )**

Thickness of hydrated bentonite layer, $t_h$	Hydration volumetric content of hydrated bentonite, $\theta_{hydr}$				Porosity of hydrated bentonite, $n_h$
	Degree of saturation of hydrated bentonite, $S_h$				
	0.7	0.8	0.9	1.0	
2 mm	< 0	< 0	< 0	< 0	0.27
$t_{hlim} = 2.43 \text{ mm}$ for $S_h = 1.0$	< 0	< 0	< 0	0.00	0.40
$t_{hlim} = 2.54 \text{ mm}$ for $S_h = 0.9$	< 0	< 0	0.00	0.04	0.43
$t_{hlim} = 2.68 \text{ mm}$ for $S_h = 0.8$	< 0	0.00	0.05	0.09	0.46
$t_{hlim} = 2.85 \text{ mm}$ for $S_h = 0.7$	0.00	0.05	0.10	0.15	0.49
3 mm	0.03	0.09	0.14	0.19	0.52
4 mm	0.20	0.26	0.33	0.39	0.64
5 mm	0.30	0.37	0.44	0.51	0.71
6 mm	0.37	0.44	0.52	0.59	0.76
7 mm	0.41	0.49	0.57	0.65	0.79
8 mm	0.45	0.53	0.61	0.70	0.82
9 mm	0.48	0.56	0.65	0.73	0.84

**Table A.3. Hydration volumetric content and porosity of hydrated bentonite as a function of the thickness of the hydrated bentonite layer and the degree of saturation of the bentonite (for  $w_0 = 15\%$ ,  $\mu_0 = 4.9 \text{ kg/m}^2 = 1 \text{ lb/ft}^2$  (i.e.  $\mu_d = 4.3 \text{ kg/m}^3 = 0.9 \text{ lb/ft}^2$ ), and  $\rho_s = 2700 \text{ kg/m}^3$ )**

Thickness of hydrated bentonite layer, $t_h$	Hydration volumetric content of hydrated bentonite, $\theta_{hydr}$				Porosity of hydrated bentonite, $n_h$
	Degree of saturation of hydrated bentonite, $S_h$				
	0.7	0.8	0.9	1.0	
2 mm	< 0	< 0	< 0	< 0	0.21
$t_{hlim} = 2.22 \text{ mm}$ for $S_h = 1.0$	< 0	< 0	< 0	0.00	0.29
$t_{hlim} = 2.29 \text{ mm}$ for $S_h = 0.9$	< 0	< 0	0.00	0.03	0.31
$t_{hlim} = 2.38 \text{ mm}$ for $S_h = 0.8$	< 0	0.00	0.03	0.07	0.34
$t_{hlim} = 2.49 \text{ mm}$ for $S_h = 0.7$	0.00	0.04	0.07	0.11	0.37
3 mm	0.12	0.17	0.21	0.26	0.47
4 mm	0.26	0.32	0.39	0.45	0.61
5 mm	0.35	0.42	0.49	0.56	0.68
6 mm	0.41	0.48	0.56	0.63	0.74
7 mm	0.45	0.53	0.61	0.68	0.77
8 mm	0.48	0.56	0.64	0.72	0.80
9 mm	0.51	0.59	0.67	0.75	0.82

given by the following equation derived from Equation A.3:

$$n_h = 1 - \frac{\mu_d}{\rho_s t_h} \quad (\text{A.15})$$

Numerical values of the porosity of the hydrated bentonite are given in the last column of each of Tables A.1 to A.3.

Tables A.1 to A.3 show that the hydration volumetric content is smaller than the porosity of the hydrated bentonite. There are two reasons for this: (i) part of the porosity is used by the initial moisture content; and (ii) part of the porosity is not used if the hydrated bentonite is not saturated. Tables A.1 to A.3 also show that the porosity and the hydration volumetric content of the hydrated bentonite vary significantly as a function of the considered parameters: for thicknesses ranging between 3 and 9 mm (which correspond to overburden pressures ranging approximately between 1000 and 0 kPa) the porosity varies approximately between 0.5 and 0.8, and the hydration volumetric content for a degree of saturation of 80% varies approximately between 0.1 and 0.6.

There is not a significant difference between the hydration volumetric content values in the three cases presented in Tables A.1 to A.3. Therefore an approximate relationship between the hydration volumetric content of the hydrated bentonite and the thickness of the hydrated bentonite layer can be developed based on Tables A.1 to A.3. This relationship is presented in Table A.4. In design calculations it is conservative to use a relatively low value of the hydration volumetric content to obtain a relatively high value of the hydrated area. Therefore the values of the hydration volumetric content presented in Table A.4 are based on relatively low values of the hydration volumetric content from Tables A.1 to A.3. Essentially, they correspond to a degree of saturation of the hydrated bentonite of approximately 0.8–0.9. Smaller values of the degree of saturation of the hydrated bentonite can be considered to achieve more conservative designs. In such cases, the hydration volumetric content should be calculated using Equations A.12 or A.13. Since the relationship presented in Table A.4 is based on Tables A.1 to A.3, it is applicable to bentonite layers having a dry mass per unit area of the

order of 3.9–4.4 kg/m<sup>2</sup> (0.8–0.9 lb/ft<sup>2</sup>). For other values of the mass per unit area of the bentonite layer, the hydration volumetric content should be calculated using Equations A.12 or A.13. The relationship between the hydration volumetric content of the hydrated bentonite and the thickness of the hydrated bentonite layer presented in Table A.4 is incorporated in Table 1 of the main text of this paper, which gives typical properties of bentonite layer relevant to design.

## APPENDIX 2. APPROXIMATE EQUATIONS

Rigorous equations for the relative hydrated area are presented in Table 3. Approximate Equations 58 to 62 are derived from the rigorous equations. The equations depend on the phase considered. The equations for the interphases (1–2 and 2–3) are simpler than the equations for the three phases. The ratio between rigorous and approximate equations are calculated below for the two interphases, and at the end of Phase 3.

The ratio between the rigorous and approximate equations at the interphase between Phases 1 and 2,  $C_{1-2}$ , is expressed as follows, based on Equations 20 and 59:

$$C_{1-2} = \frac{W_P}{W_P - B_o} + \frac{W_P}{L_P - B_o} - \frac{B_o W_P}{(W_P - B_o)(L_P - B_o)} \quad (\text{A.16})$$

Hence:

$$C_{1-2} = \frac{1}{1 - (B_o/W_P)} + \frac{1}{(L_P/W_P) - (B_o/W_P)} - \frac{(B_o/W_P)}{[1 - (B_o/W_P)][(L_P/W_P) - (B_o/W_P)]} \quad (\text{A.17})$$

The ratio between the rigorous and approximate equations at the interphase between Phases 2 and 3,  $C_{2-3}$ , is expressed as follows, based on Equations 21 and 61:

$$C_{2-3} = \frac{W_P}{W_P - B_o} + \frac{W_P}{L_P - B_o} - \frac{2B_o W_P}{(W_P - B_o)(L_P - B_o)} \quad (\text{A.18})$$

Hence:

$$C_{2-3} = \frac{1}{1 - (B_o/W_P)} + \frac{1}{(L_P/W_P) - (B_o/W_P)} - \frac{(2B_o/W_P)}{[1 - (B_o/W_P)][(L_P/W_P) - (B_o/W_P)]} \quad (\text{A.19})$$

It should be noted that the equations for  $C_{1-2}$  and  $C_{2-3}$  are similar. The only difference is a factor 2 in the third term. Since this term is small compared with the two other terms, the difference between  $C_{1-2}$  and  $C_{2-3}$  is small. Hence:

$$C_{1-2} \approx C_{2-3} \approx C_{RHA} \quad (\text{A.20})$$

Numerical calculations confirm that the difference between  $C_{1-2}$  and  $C_{2-3}$  is small, and give the approximate values presented in Table 5.

**Table A.4. Relationship between hydration volumetric content of hydrated bentonite and thickness of hydrated bentonite layer (for dry mass per unit area of the order of 3.9–4.4 kg/m<sup>2</sup> (0.8–0.9 lb/ft<sup>2</sup>) and initial moisture content ranging between 15 and 25%)**

Thickness of hydrated bentonite layer, $t_h$ (mm)	Hydration volumetric content of hydrated bentonite, $\theta_{hydr}$ (dimensionless)
8.0	0.50
7.0	0.45
6.0	0.40
5.0	0.35
4.0	0.25
3.5	0.15

Based on the foregoing demonstration, the dimensionless factor  $C_{RHA}$  is valid only for Phases 1 and 2. In Phase 3, a new factor,  $C_{RHA3}$ , should be used (Equation 67). This factor varies from the value of  $C_{RHA}$  at the beginning of Phase 3 to the value  $C_{RHAend}$  at the end of Phase 3. The value of  $C_{RHAend}$  is established as follows by calculating the ratio of Equations 22 and 62:

$$C_{RHAend} = \frac{1}{(2/W_P) \left[ \sqrt{3B_o^2 + (2k\hat{t}\Delta h/\theta_{hydr})} - 2B_o \right]} \quad (A.21)$$

Combining Equations 14, 54 and A.21 gives

$$C_{RHAend} = \frac{W_P}{W_P - B_o} \quad (A.22)$$

For  $W_P = 5.3$  m,  $C_{RHAend}$  has the values given in the last column of Table 5.

An example of use of the dimensionless factors  $C_{RHA}$  and  $C_{RHAend}$  is given in Example 1 in Section 4.2.

### APPENDIX 3. ERRATA FOR PREVIOUSLY PUBLISHED PAPER

As indicated in the Acknowledgements section, this paper is an expanded version of a previously published paper (Giroud *et al.* 2002). The previously published paper contained some errors:

Equation 39 of the previously published paper is incorrect ( $L$  is missing). The correct equation is Equation 41 in this paper.

Equation 41 of the previously published paper is incorrect (the differential term is repeated). The correct equation is Equation 43 in this paper.

Equation 47 of the previously published paper contains a typographical error. The correct equation is Equation 50 in this paper.

The explanation that precedes equation 51 in the previously published paper is incomplete. For that equation to be valid it is also necessary that the time,  $\hat{t}$ , be sufficiently large to ensure that  $B_o$  is small with respect to the square root. Practically, equation 51 of the previously published paper is applicable only when the time is extremely large. Therefore the use of equation 51 of the previously published paper is not recommended. As a result, the comment based on equation 51 presented after table 1 of the previously published paper is not appropriate.

There are incorrect lines on the left side of figures 3a, 3b and 3c of the previously published paper. The correct figure is Figure 6 of this paper.

Finally, and perhaps more importantly, the equations of the previously published paper were written in terms of effective porosity, which is not appropriate. Instead, in the present paper, the equations are written in terms of hydration volumetric content, which is more correct. Therefore the authors recommend the equations of the present paper and not those of the previously published paper.

### NOTATIONS

Basic SI units are given in parentheses.

$A$	cross-sectional area through which liquid is migrating ( $m^2$ )
$A_o$	cross-sectional area through which liquid is migrating in overlap ( $m^2$ )
$A_e$	cross-sectional area through which liquid is migrating beyond overlap ( $m^2$ )
$A_H$	hydrated area of a panel due to water migrating through overlaps of GM-GCL panels ( $m^2$ )
$A_{Hdef}$	hydrated area due to liquid migrating through geomembrane defect ( $m^2$ )
$A_P$	effective panel area ( $m^2$ )
$A_U$	unhydrated area of a panel ( $m^2$ )
$A_{unit}$	unit area ( $m^2$ )
$a$	area of geomembrane circular defect ( $m^2$ )
$A/L$	cross-sectional area through which liquid is migrating, per unit length perpendicular to plane of Figure 6 or 7 (m)
$A_o/L$	cross-sectional area through which liquid is migrating in overlap, per unit length perpendicular to plane of Figure 6 or 7 (m)
$A_e/L$	cross-sectional area through which liquid is migrating beyond overlap, per unit length perpendicular to plane of Figure 6 or 7 (m)
$B$	distance reached by water beyond overlap (m)
$B_1$	width of bentonite within overlap that is hydrated at a given time during Phase 1 (m)
$B_o$	overlap width (m)
$C_{RHA}$	factor in approximate equations for relative hydrated area in Phases 1 and 2 (dimensionless)
$C_{RHA3}$	factor in approximate equation for relative hydrated area in Phase 3 (dimensionless)
$C_{RHAend}$	value of $C_{RHA3}$ at end of Phase 3 (dimensionless)
$h$	head (m)
$h_s$	pressure head in soil underlying lower geomembrane (m)
$h_w$	head of liquid above a defect in upper geomembrane (m)
$\Delta h$	head difference, given by Equation 2, 3 or 4 depending on mode of liquid migration considered (m)
$\Delta h_o$	head loss in overlap (m)
$\Delta h_e$	head loss in bentonite section hydrated beyond overlap (m)
$i$	hydraulic gradient (dimensionless)
$i_1$	hydraulic gradient in Phase 1 (dimensionless)
$i_o$	hydraulic gradient in overlap (dimensionless)
$i_e$	hydraulic gradient in bentonite section hydrated beyond overlap (dimensionless)
$k$	hydraulic conductivity of (hydrated) bentonite (m/s)
$L$	length, measured perpendicular to plane of Figure 6 or 7 (m)
$L_P$	panel length (m)
$L_P - B_o$	effective panel length (m)

$N$	number of defects in the considered unit area (dimensionless)	$W_H$	width of hydrated area in one panel (m)
$n$	porosity of bentonite (dimensionless)	$W_P$	panel width (m)
$n_h$	porosity of hydrated bentonite (dimensionless)	$W_P - B_o$	effective panel width (m)
$Q$	rate of liquid migration ( $m^3/s$ )	$w$	moisture content of bentonite (dimensionless)
$Q/L$	rate of liquid migration per unit length perpendicular to plane of Figure 6 or 7 ( $m^2/s$ )	$w_0$	initial moisture content of bentonite (dimensionless)
$R$	radial distance between center of upper geomembrane defect and hydration front in case of liquid migrating through a geomembrane defect (m)	$w_h$	moisture content of hydrated bentonite (dimensionless)
$R_{HA}$	relative hydrated area, defined as ratio between hydrated area and effective panel area (dimensionless)	$w_{sath}$	saturated moisture content of hydrated bentonite (i.e. moisture content that hydrated bentonite would have if it were saturated without volume change between hydrated state and saturated state) (dimensionless)
$R_{HA1}$	relative hydrated area in Phase 1 (dimensionless)	$\theta$	volumetric moisture content of bentonite (dimensionless)
$R_{HA1-2}$	relative hydrated area at Interphase 1–2 (i.e. at end of Phase 1 and beginning of Phase 2) (dimensionless)	$\theta_{hydr}$	hydration volumetric content (i.e. volumetric content of water used to hydrate bentonite) (dimensionless)
$R_{HA2}$	relative hydrated area in Phase 2 (dimensionless)	$\mu$	mass per unit area of bentonite layer ( $kg/m^2$ )
$R_{HA2-3}$	relative hydrated area at Interphase 2–3 (i.e. at end of Phase 2 and beginning of Phase 3) (dimensionless)	$\mu_0$	initial mass per unit area of bentonite layer ( $kg/m^2$ )
$R_{HA3}$	relative hydrated area in Phase 3 (dimensionless)	$\mu_d$	dry mass per unit area of bentonite layer (i.e. mass per unit area of the dry bentonite layer) ( $kg/m^2$ )
$R_{HAend}$	relative hydrated area at end of Phase 3 (i.e. when the entire panel is hydrated) (dimensionless)	$\mu_h$	mass per unit area of hydrated bentonite layer ( $kg/m^2$ )
$R_{HAdef}$	relative hydrated area due to geomembrane defect (dimensionless)	$\mu_w$	initial mass per unit area of water added for hydration ( $kg/m^2$ )
$r$	radius of geomembrane defect (m)	$\rho$	density ( $kg/m^3$ )
$S_h$	degree of saturation of hydrated bentonite (dimensionless)	$\rho_s$	density of bentonite particles ( $kg/m^3$ )
$s_b$	suction head in bentonite at hydration front (m)	$\rho_w$	density of water ( $kg/m^3$ )
$s_s$	suction head in soil underlying lower geomembrane (m)	$\sigma$	normal stress (Pa)
$t$	thickness of bentonite layer (m)	$\tau$	shear strength (Pa)
$t_0$	initial thickness of bentonite layer (m)	$\tau_{dry}$	shear strength of dry bentonite (Pa)
$t_h$	thickness of hydrated bentonite layer (m)	$\tau_{hydr}$	shear strength of hydrated bentonite (Pa)
$t_{hlim}$	limit value of hydrated bentonite layer thickness below which hydration volumetric content is negative (m)	$\tau_{peak-dry}$	peak shear strength of dry bentonite (Pa)
$t_w$	equivalent thickness of water added for hydration (m)	$\tau_{peak-hydr}$	peak shear strength of hydrated bentonite (Pa)
$\hat{t}$	time (s)	$\tau_{prorated}$	prorated shear strength (Pa)
$\hat{t}_1$	time during Phase 1 (s)	$\tau_{residual-dry}$	residual shear strength of dry bentonite (Pa)
$\hat{t}_{1-2}$	time at Interphase 1–2, i.e. at end of Phase 1 and beginning of Phase 2 (s)	$\tau_{residual-hydr}$	residual shear strength of hydrated bentonite (Pa)
$\hat{t}_2$	time during Phase 2 (s)		
$\hat{t}_{2-3}$	time at Interphase 2–3, i.e. at end of Phase 2 and beginning of Phase 3 (s)		
$\hat{t}_3$	time during Phase 3 (s)		
$\hat{t}_{end}$	time at which entire bentonite layer is hydrated, i.e. at end of Phase 3 (s)		
$V$	volume of liquid used to hydrate bentonite layer between time zero ( $\hat{t} = 0$ ) and time $\hat{t}$ ( $m^3$ )		
$V/L$	volume of liquid used to hydrate the bentonite layer between time zero ( $\hat{t} = 0$ ) and time $\hat{t}$ per unit length perpendicular to the plane of Figure 6 or 7 ( $m^2$ )		

## REFERENCES

- Daniel, D. E. Results of shear strength tests on the bentonite component of partly wetted Gundseal GCL. Letter dated 22 February 1993 to J. Anderson of Gundle Lining Systems. Personal communication.
- Daniel, D. E. (1996) Geosynthetic clay liners. Part Two: Hydraulic properties. *Geotechnical Fabrics Report*, **14**, No. 5, 22–26.
- Estornell, P. & Daniel, D. E. (1992). Hydraulic conductivity of three geosynthetic clay liners. *Journal of Geotechnical Engineering*, **118**, No. 10, 1592–1606.
- Giroud, J. P. & Daniel, D. E. (2004). Liquid migration in an encapsulated bentonite layer due to geomembrane defects. *Geosynthetics International*, **11**, No. 4, 311–329.
- Giroud, J. P., Thiel, R. S., Kavazanjian, E. & Lauro, F. J. (2002). Hydrated area of a bentonite layer encapsulated between two geomembranes. *Proceedings of the 7th International Conference on Geosynthetics*, Nice, France, Balkema, Lisse, The Netherlands, Vol. 2, pp. 827–832.
- Green, W. J. & Ampt, G. A. (1911). Studies on soil physics. Part I: The flow of air and water through soils. *Journal of Agricultural Science*, **4**, 1–24.

- Kavazanjian, E. (1999). Seismic design of solid waste containment facilities. *Proceedings of the 8th Canadian Conference on Earthquake Engineering*, Vancouver, British Columbia, pp. 51–68.
- Sabatini, P. J., Griffin, L. M., Bonaparte, R., Espinoza, R. D. & Giroud, J. P. (2001). Reliability of state of practice for selection of shear strength parameters for waste containment system stability analyses. *Proceedings of the 15th Annual GRI Conference*, Geosynthetics Research Institute, Drexel University, Philadelphia, pp. 86–109.
- Sabatini, P. J., Griffin, L. M., Bonaparte, R., Espinoza, R. D. & Giroud, J. P. (2002). Reliability of state of practice for selection of shear strength parameters for waste containment system stability analyses. *Geotextiles and Geomembranes*, **20**, No. 4, 241–262.
- Shan, H. Y. (1993). *Stability of Final Covers Placed on Slopes Containing Geosynthetic Clay Liners*, PhD dissertation, University of Texas, Austin, 296 pp.
- Stark, T. D. & Eid, H. T. (1994). Drained residual strength of cohesive soils. *Journal of the Geotechnical Engineering Division, ASCE*, **120**, No. 5, 856–871.
- Thiel, R. S., Daniel, D. E., Erickson, R. B., Kavazanjian, E. & Giroud, J. P. (2001). *The GSE GundSeal GCL Design Manual*. Gundle/SLT Environmental, Inc., Houston, Texas, USA.
- Watry, S. M. & Lade, P. V. (2000). Residual shear strengths of bentonites on the Palos Verdes Peninsula, California. In *Slope Stability 2000* (eds D. V. Griffin, G. A. Fenton and T. R. Martin), ASCE Geotechnical Special Publication No. 101, pp. 323–342.

**The Editors welcome discussion in all papers published in Geosynthetics International. Please email your contribution to [discussion@geosynthetics-international.com](mailto:discussion@geosynthetics-international.com) by 15 February 2005.**